JANEK UIN

Electrical separation
for generating standard aerosols
in a wide particle size range

This study was carried out at the University of Tartu, Estonia.

This dissertation was admitted on June 17, 2011, in partial fulfilment of the requirements for the degree of Doctor of Philosophy in physics (applied physics) and was allowed for defence by the Council of the Institute of Physics, University of Tartu.

Supervisors: Eduard Tamm, PhD, University of Tartu, Estonia
Aadu Mirme, PhD, University of Tartu, Estonia

Opponents: Prof. Jyrki Mäkelä, PhD, Tampere University of Technology, Finland
Veljo Kimmel, PhD, Estonian University of Life Sciences, Estonia

Defence: August 22, 2011, at the University of Tartu, Estonia

Contents

List of publications

This thesis is based upon the following publications (full texts included at the end), which are referred to in the text by their Roman numerals:

I Uin, J., Tamm, E. (2010). Assessment of the quality of electrically produced standard aerosols. *Aerosol and Air Quality Research*, 10, 609 – 615.

II Uin, J., Tamm, E., Mirme, A. (2009). Electrically Produced Standard Aerosols in a Wide Size Range. *Aerosol Science and Technology*, 43, 847 – 853.

III Uin, J., Tamm, E., Mirme, A. (2011). Very Long DMA for the generation of the calibration aerosols in particle diameter range up to 10 µm by electrical separation. *Aerosol and Air Quality Research*, accepted for publication on 20.06.2011.

IV Uin, J., Mirme, S., Mirme, A., Tamm, E. (2006). Comparison of the performance of modified Vienna type DMA and TSI nano-DMA. *Chemical Engineering Transactions*, 10, 173 – 177.

V Mirme, A., Tamm, E., Mordas, G., Vana, M., Uin, J., Mirme, S., Bernotas, T., Laakso, L., Hirsikko, A., Kulmala, M. (2007). A wide range multi-channel Air Ion Spectrometer. *Boreal Environment Research*, 12, 247 – 264.

Other publications, not directly included in this thesis:

VI Uin, J., Tamm, E. (2010). Effect of gravity on electrical separation of the aerosol particles in diameter range up to 10 µm, Abstract 1180. *International Aerosol Conference 2010*; Helsinki, Finland, 29 August – 03 September 2010, Abstract 1180.

VII Uin, J., Tamm, E. (2009). Distortions of the DMA transfer function due to geometrical and flow pattern non-ideality and gravity. *European Aerosol Conference 2009*, Karlsruhe, Germany, 6 – 11 September 2009, Abstract T096A02.

VIII Uin, J., Tamm, E. (2008). Assessment of the quality of electrically produced standard aerosols. *European Aerosol Conference 2008*, Thessaloniki, Greece, 25-29 August 2008, Abstract T04A048P.

IX Uin, J., Mirme, A., Mirme, S., Tamm, E. (2007). Generation of standard aerosols by electrical separation in a wide size range. *European Aerosol Conference 2007*, Salzburg, Austria, 9 – 14 September 2007, Abstract T02A035.

X Mirme, S., Mirme, A., Tamm, E., Uin, J. (2007). Evaluation of Neutral Cluster and Air Ion Spectrometer (NAIS). *European Aerosol Conference 2007*, Salzburg, Austria, 9 – 14 September 2007, Abstract T02A021.

XI Mirme, S., Uin, J., Tamm, E., Mirme, A. (2006). Charging of aerosol in engine exhaust particle sizer (EEPS). *Proceedings of the 7th International Aerosol Conference*, 7th International Aerosol Conference, St. Paul, MN, USA, 10 – 15 September 2006, 630 – 631.

XII Asmi, E., Sipilä, M., Manninen, H. E., Vanhanen, J., Lehtipalo, K., Gagné, S., Neitola, K., Mirme, A., Mirme, S., Tamm, E., Uin, J., Komsaare, K., Attoui, M., Kulmala, M. (2009). Results of the first air ion spectrometer calibration and intercomparison workshop. *Atmospheric Chemistry and Physics*, 9, 141 – 154.

XIII Kerminen, V.-M. , Lihavainen, H., Brus, D., Asmi, E., Sipilä, M., Manninen, H. E., Kurten, T., Vehkamäki, H., Ortega, I. K., Mirme, A., Mirme, S., Uin, J. , Hõrrak, U., Berndt, T., Stratmann, F., Lehtinen, K., Baltensperger, U., Laaksonen, A., Kulmala, M. (2009). Nucleation Studies within the EUCAARI Project. *18th International Conference on Nucleation and Atmospheric Aerosols*, Prague, Czech Republic, 10 – 14 August 2009, 322 – 325.

XIV Kerminen, V-M., Asmi, E., Brus, D., Sipilä, M., Manninen, H., Kurtén, T., Vehkamäki, H., Ortega, I., Mirme, A., Mirme, S., Uin, J., Hõrrak, U., Berndt, T., Stratmann, F., Laaksonen, A., Kulmala, M. (2008). 1. Emission and formation element. WP1.1: Nucleation (EUCAARI work package abstracts). *Proceedings of 2008 EUCAARI Annual Meeting*, Helsinki, Finland, 17 – 21 November 2008, (Report Series in Aerosol Science, 99), 11 – 15.

Author's contributions

The author of this thesis was responsible for the following work, presented in the main publications [I-IV] listed above:

- [I]: writing the software and running the calculations for standard aerosol quality, analyzing the results. Conducting the experiments for

determining the standard aerosol quality and analyzing the results. Writing the manuscript text.

- [II]: performing the experiments for assessing the new method for standard aerosol generation, writing the software for automatic control of the experimental setup, running the calculations and analyzing the results. Writing 2/3 of the manuscript text.

- [III]: writing the software and running the calculations for the theoretical DMA transfer function. Conducting the experiments for measuring the actual DMA transfer function. Writing 1/3 of the manuscript text.

- [IV]: writing the software for controlling the instruments, performing the experiments for determining the transfer functions of DMAs and analyzing the results. Writing the manuscript text.

- [V]: managing the experimental setup for standard aerosol generation for the Estonian part of the instrument calibration campaign. Writing a part of the manuscript text (approximately 1/10), including two figures.

Abstract

The main subject of this thesis is the generation of standard aerosols for instrument calibration by means of electrical separation of charged aerosol particles. The need for instrument calibration and the methods for doing it are briefly discussed. Then, electrical separation as one of the means for producing aerosols for instrument calibration is examined in more detail. An overview of the method is given and challenges in using it are described. The problem of multiple charges, when using electrical methods for standard aerosol generation, is examined. From this, a parameter for describing an electrically generated standard aerosol – aerosol quality – is presented. Dependence of the quality on several initial parameters of aerosol generation process is examined with a conclusion, that obtaining high quality by conventional means can be difficult. Next, a method for obtaining higher quality standard aerosol is presented and described in detail. It is experimentally shown that this method allows reliably to obtain high quality standard aerosols in a wide particle size range. A design of a Differential Mobility Analyzer is briefly described that makes it possible to use the previously described method for standard aerosol generation with larger aerosol particles. The performance of the DMA is evaluated both theoretically and experimentally and it is found to be within expected margins. A new method, using monodisperse polymer size standards for the assessment of the main characteristic of the DMA – its transfer function – is described for the large particle region.

1 Introduction

Aerosols are the research objects for many fields of science and technology. Various behavior aspects of very different natural and laboratory-made aerosols are being investigated but, however, the actual aerosol parameters under study are usually either the mass- or number concentration or the aerosol particle size. Among these, the particle size is an important parameter as it determines a lot of the particles' properties; thus, knowing the size distribution of the particles of an aerosol is essential for many cases.

Methods for determining the aerosol size distribution are numerous (Willeke & Baron, 1993), but can generally be divided into two categories: methods based on aerosol collection and the later analysis of the deposit, and those that use the real-time in-situ measurements. Instruments using the latter method produce some kind of a signal in response to the value of an aerosol property being measured, which is tied to the particle size. To provide a link between the instrument response and the particle size, calibration of the instrument is needed. This requires an etalon, an aerosol with well-known properties, i.e. a well-determined particle size spectrum – a standard aerosol.

There exist several methods for standard aerosol generation, the most well-known among them being the following.

1. The pneumatic pulverization of the aqueous suspension of monodisperse nano- and microspheres (Raabe, 1968) produces droplets containing monodispersed polymer (latex) particles that are used as a size standard after the droplets have been dried (see also section 5). These are used mainly for calibrating optical instruments as the particle concentrations tend to be too low for many instruments using the electrical methods.

2. The pulverization of non-volatile liquids or solutions by vibrating orifice generators (Berglund & Liu, 1973) that produce highly monodisperse droplets with sizes starting from about 1 micrometer (smaller particle sizes can be achieved by using volatile mixtures and later drying the droplets). With this method it is often difficult to obtain the right working regime for the generator so that *only* the desired particles are produced.

3. The electrical separation of particles from a polydisperse aerosol (Liu & Pui, 1974) or from the electrospray of the solution of some large-molecule organic substances (Ude & Fernandez de la Mora, 2005). The latter produces standard aerosols with very narrow size distribu-

tions as the individual aerosol particles consist only of one molecule of the working substance. For the same reason this method can only be used for generating particles in the size range of a few nanometers.

The described methods are generally limited in their usability outside specific particle size ranges. The method of electrical separation from polydisperse aerosols, despite its own shortcomings, can possibly be considered the most versatile, as it can be more easily applied in a wide particle size range.

2 Electrical separation

2.1 Electrical separator – DMA

Electrical separation, developed by Liu & Pui (1974) is a method for extracting from the polydisperse aerosol (primary aerosol – PA) a narrow fraction according to the particles' electrical mobility (secondary aerosol – SA). This process is realized in an electrical classifier (separator, Differential Mobility Analyzer – DMA)(Knutson & Whitby, 1975).

According to Tammet (1970), Differential Mobility Analyzer can be classified as a second order aspiration capacitor with divided input and output air flows. Schematic diagram of the most common Hewitt type DMA (Hewitt, 1957) is depicted in Figure 1. It consists of two concentric cylindrical electrodes. The outer cylindrical electrode has a narrow annular opening where the aerosol being separated enters with flow rate Φ_2. Filtered sheath air flows between the two electrodes carrying the aerosol particles along the axis of the DMA; it enters with the flow rate Φ_1. Radial electric field is applied between the electrodes that causes the charged aerosol particles to drift towards the inner electrode with a velocity proportional to their electrical mobility. Particles with mobilities in a certain narrow range reach the annular output opening in the inner electrode and are drawn out of the DMA, together with a part of the sheath air, with the flow rate Φ_3. Excess air is drawn out with the flow rate Φ_4

Depending on the vertical positions on the input and output openings between which an aerosol particle travelled, four distinct limiting surfaces (made up by the trajectories of particles) can be identified, denoted in Figure 1 with dashed lines. Particles travelling along these trajectories have limiting mobilities k_j ($j =$1, 2, 3, 4):

$$k_j = \frac{\varepsilon_0 \Phi^j}{CU} \, ,\tag{1}$$

where U is the voltage between the electrodes of the DMA, C is the active capacitance (i.e. the capacitance of the part between the input and the output opening) and ε_0 is the electric constant. Φ^j denotes the total airflow that passed through a limiting surface (formed by the trajectories of particles with the limiting mobility k_j) e.g. $\Phi^1 = \Phi_1 + \Phi_2 - \Phi_3$.

The main characteristic of the separator is the particle size spectrum of its output aerosol. In case of lack of the interaction between particles in the DMA, the density function $\varphi(k)$ of the particle mobility number spectrum of the separated aerosol is proportional to the corresponding density function $f(k)$ of the aerosol being separated:
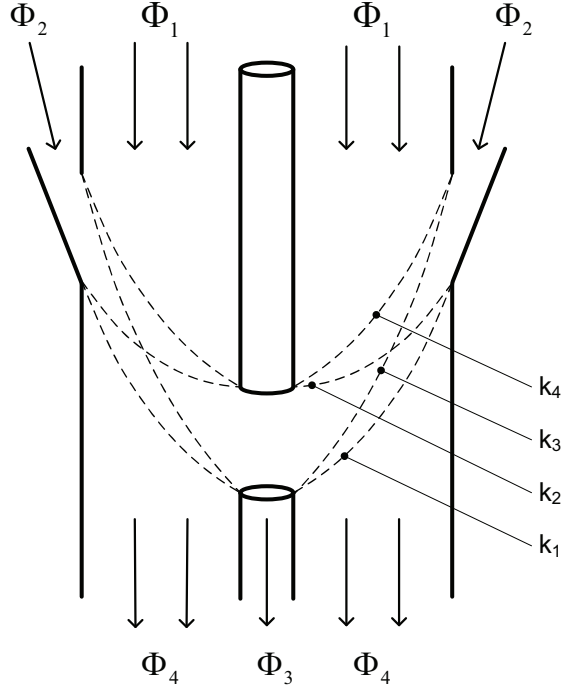
Figure 1: Simplified schematic of the Hewitt-type Differential Mobility Analyzer.

$$\varphi(k) = H(k)f(k). \tag{2}$$

$H(k)$ is the separator's dimensionless transfer function, describing physical processes in the DMA. In case of ideal geometry and exactly laminar flows, which are uniformly distributed over the perimeter of the annular space between the electrodes, and also choosing $\Phi_2 = \Phi_3$, $H(k)$ has a triangular form (Tammet, 1970; Hoppel, 1978):

$$H(k) = \begin{cases} 0 & k < k_3 \\ \left(\frac{k}{k_1} - 1\right)\frac{\Phi_1}{\Phi_3} + 1 & k_3 < k < k_1 \\ 1 & k = k_1 \\ \left(1 - \frac{k}{k_1}\right)\frac{\Phi_1}{\Phi_3} + 1 & k_1 < k < k_2 \\ 0 & k > k_2 \end{cases}. \tag{3}$$

To make computations simpler (see, for example, section 3.2), the previous equation can be rewritten as (Stolzenburg, 1988; Stratmann et al., 1997):

Figure 2: Triangular transfer function of a DMA.

$$H(k, k') = \frac{\alpha}{2\beta} \left(\left| \frac{k}{k'} - (1 + \beta) \right| + \left| \frac{k}{k'} - (1 - \beta) \right| - 2 \left| \frac{k}{k'} - 1 \right| \right). \quad (4)$$

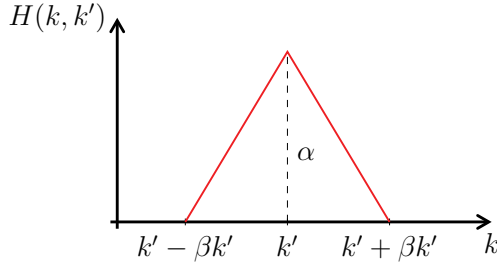Here, the transfer function H is written as a function of its midpoint mobility $k' = k_1 = k_4$ ($\Phi_2 = \Phi_3$ was chosen). Also two empirical parameters are introduced: the height of the transfer function α (mostly equal to 1) and the relative half-width $\beta = \Phi_3/\Phi_1$ (Figure 2). Concentration of SA particles at the outlet of the DMA (for a given k') is expressed by an integral:

$$n(k') = \int H(k, k') f(k) \mathrm{d}k. \quad (5)$$

Deflections from ideal conditions and the diffusion of (small) particles distort the shape of the transfer function – it becomes bell-shaped; greater deflections create an asymmetry of the bell or even a bimodal shape of the transfer function(Chen & Pui, 1997; Stratmann et al., 1997; Mamakos et al., 2007; Stolzenburg & McMurry, 2008). The above statements are correct for small particles. In case of large particles, when the particle's settling velocity in the gravitational field is comparable with its velocity in the electric field of the DMA, the effect of gravity must be considered [V](Bronec et al., 1999).

2.2 The multiple charge problem

To use the method of electrical separation, at least some of the particles of PA must be charged electrically as uniformly as possible (their charge must be independent of their diameter) – then the extracted fraction of particles, narrow according to their electrical mobilities, is narrow by the particle size as well. Uniform charging of the particles is a rather complicated problem. For small particles (diameter $d < 40$ nm) the problem can be solved by exposing the particles to a symmetrically bipolar ion atmosphere. There

the particles obtain a stationary charge distribution, with the probability of more than one electron charge on a particle being negligible for such small particles (Fuchs, 1947, 1963). Now the particle mean diameter and the width of the size spectrum of SA can be found, knowing the geometric and regime parameters of the DMA (which define its transfer function), e.g. via Equation (2) (assuming that $H(k)$ is much narrower than $f(k)$, so that $f(k) \approx const$ could be considered). Particle concentration can be determined by measuring the electric current carried by the singly charged particles to some current sensor.

In case of larger particles ($d > 40$ nm and especially when $d \gg 40$ nm), an aerosol with a stationary charge distribution includes multiply charged particle fractions. This means that among the separated particles with a narrow mobility distribution there are multiply charged larger particles, having the same mobility as the singly charged "major" particles. As a result, SA with an asymmetric or even multimodal size distribution is obtained, which is not well suited for using as a standard aerosol (Kikas et al., 1982; Reischl, 1991; Tamm, 1992). The effect of the multiply charged particles can be suppressed by several methods: shifting the point of separation in the particle diameter scale (see below), by narrowing the particle charge distribution in comparison with the stationary distribution (Gupta & Mc-Murry, 1989; Peil et al., 1992), by decreasing the ion concentration at the charging stage (Han et al., 2003) or by removing large particles with multiple charges using an inertial impactor (Romay-Novas, 1988). However, a full solution to the problem cannot be achieved this way. The presence of multiple size fractions in SA decreases its usability as a standard aerosol and it can be said that the "quality" of the standard aerosol has decreased. To illustrate this better, a theoretical situation is constructed next where SA is separated from PA with multiple differently charged size fractions.

As PA is a fresh aerosol from a generator, its size distribution (density) function (size spectrum)[1] $f(d)$ may be considered lognormal (Fuchs, 1964; Hinds, 1999):

$$f(d) = \frac{N}{\sqrt{2\pi}\, d \ln \sigma_g} \exp\left(-\frac{\ln^2 \frac{d}{d_g}}{2\ln^2 \sigma_g} \right), \qquad (6)$$

where d_g and σ_g are the geometric mean diameter and the geometric standard deviation, accordingly, and N is the total number concentration of particles. In case of a stationary charge distribution, the mobility distribution function $f(k)$ of PA is comprised of several components $f^i(k)$,

_____

[1]The size or mobility distribution of the particle number concentration is used everywhere, unless noted otherwise
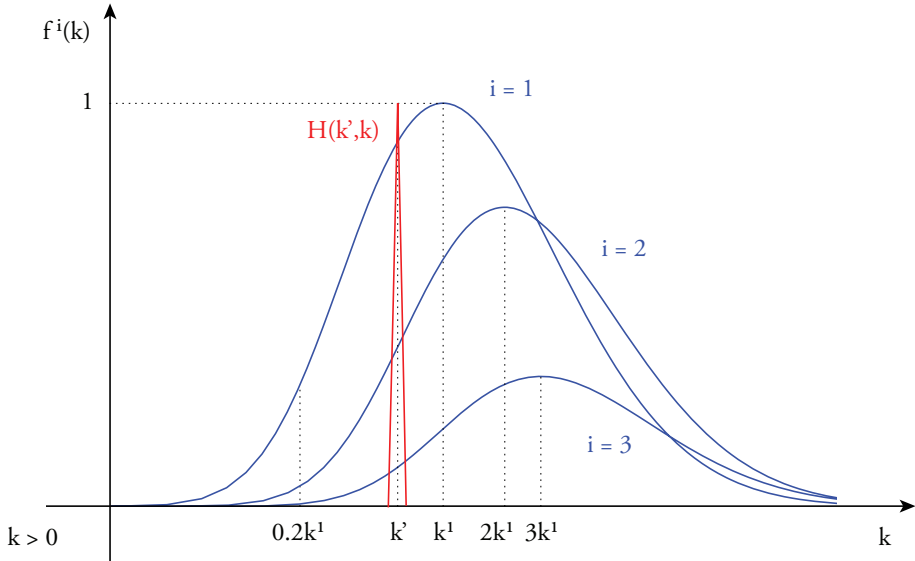
Figure 3: Mobility distribution function of 1-, 2- and 3-fold charged components of PA (with a stationary charge distribution) and the triangular DMA transfer function H (with the relative half-width of 0.1) in logarithmic mobility scale. All the curves are rescaled so that the singly charged component has a unit height. The vertical axis is positioned at $k > 0$ and $k' = 0.6k^1$.

describing i-fold charged particles. This is illustrated in Figure 3, where differently charged components of PA, derived from a lognormal size distribution with $d_g = 200$ nm and $\sigma_g = 2.2$ (the last value is typical for pneumatic atomization generators) are presented along with a triangular DMA transfer function H.

As it can be seen from Figure 3, the different PA components overlap in the mobility scale. This means that the concentrations of differently charged particles and the overall concentration of SA are determined by the properties of the PA distribution, i.e. the given d_g and σ_g, and by the position k' of the peak (and to a lesser degree also the width) of the DMA transfer function $H(k, k')$ (Equation (5)). With a given PA distribution, moving k' towards lower mobilities increases the relative amount of singly charged particles in SA while the overall SA concentration decreases.

3 Standard aerosol quality

3.1 Definition of quality

As described above, the presence of multiple charges on SA can severely limit its usability as a standard aerosol. In order to quantify how well suited a particular SA is for being a standard aerosol, a parameter called "quality" is defined as the amount of singly charged particles in relation to all charged particles in the electrically separated aerosol[2] [I]:

$$\xi = \frac{n_1}{n} = \frac{n_1}{\sum_{i>0} n_i} \,,$$

(7)

where n is the total number concentration of all charged particles (of one sign) and n_1 and n_i are the number concentrations of particles with 1 and i charge(s) of the same sign, accordingly. The parameter ξ takes values from 0 (no singly charged particles) to 1 (all charged particles are singly charged), the latter being the ideal case and thus desirable for a standard aerosol.

From Figure 3 in the previous paragraph, it was seen that the amount of differently charged particles in SA and thus its quality are dependent on the parameters of the PA distribution function and the transfer function of the electrical separator (DMA). Considering the definition of a DMA transfer function, the mobility distribution density $\varphi(k)$ of SA can be written as (slightly different form of Equation (2)):

$$\varphi(k) = H(k, k')f(k) \,.$$

(8)

From here the concentration of particles in SA having i charges can be found:

$$n_i = \int_{k_3}^{k_2} H(k, k')f^i(k)\mathrm{d}k \,,$$

(9)

where $f^i(k)$ is the mobility distribution function of particles with i charges in PA and $k_3 = (1 - \beta)k'$ and $k_2 = (1 + \beta)k'$ are the limiting mobilities of the transfer function (see also section 2.1). In the particle diameter scale this can be written as

$$\frac{n_i}{N} = \int_{d(k_2)}^{d(k_3)} H\left(d, d(k')\right) f^{*i}(d)\mathrm{d}d = \int_{d(k_2)}^{d(k_3)} H\left(d, d(k')\right) p_i(d) f^*(d)\mathrm{d}d \,.$$

(10)

---

[2]As electrical separation deals with one polarity at a time, everywhere only one charge sign is being considered, unless noted otherwise.

Here $f^*(d) = f(d)/N$ is the distribution function (Equation (6)) of all particles and $f^{*i}(d)$ is the distribution function of particles with i charges in PA, both normalized to 1. The parameter $p_i(d)$ is the probability for i charges on particles with a given diameter as obtained by the Fuchs algorithm (Fuchs, 1947) with corrections by Tammet (Tammet, 1991; Hõrrak et al., 1998).

Using Equations (6), (7) and (10) and varying the value of i, the SA quality ξ and $n_N = n/N$, the relative concentration of all charged particles (of the same sign) in the SA, can be calculated as a function of PA parameters d_g and σ_g (complete description of the algorithm is given in appendix C.1 on page 48).

3.2 Example results of calculations

Example calculations of the SA quality where done for two different cases. First, the situation where SA is separated from the peak of the PA distribution, i.e. $k' = k^1$, was examined. Next, the k' was shifted towards the lower mobility end of the distribution and the calculations were repeated. For this a new "shift-parameter" $\gamma = 0 \ldots 1$ was introduced so that $k' = \gamma k^1$.

For these calculations the DMA transfer function $H(k, k')$ in Equation (10) was assumed to be triangular (see section 2.1). For the two transfer function parameters – the height α and relative half-width β, the actual set of values from previous experiments (see also appendix B)[IV] was used, however, no significant difference was observed compared to the ideal case where $\alpha = 1$ and $\beta = 0.1$ (with aerosol- to sheath air flow rate ratio of 1/10).

Calculation results are shown in Figure 4. As it can be seen from the first graph (a), when separating from the peak of the distribution, the SA quality decreases rapidly when particle size gets higher than about 50 nm. A good quality at these larger particle sizes would be attainable only with unrealistically low values of σ_g. One method to remedy this situation has been to separate from the lower mobility end of the PA distribution, trying to avoid multiply charged particles (see Figure 3 on page 17). The second graph (b) illustrates this case. From the graph it is visible that not much improvement can actually be made this way – the quality of SA is higher, but the gain is relatively small. Also, as expected, the resulting particle concentrations are much lower compared to those obtainable when separating from the peak: the relative concentration n_N of particles in SA differs approximately five times.

The graphs in Figure 4 also show that the general decrease in quality with an increasing d_g is not monotonic: a region of especially low quality
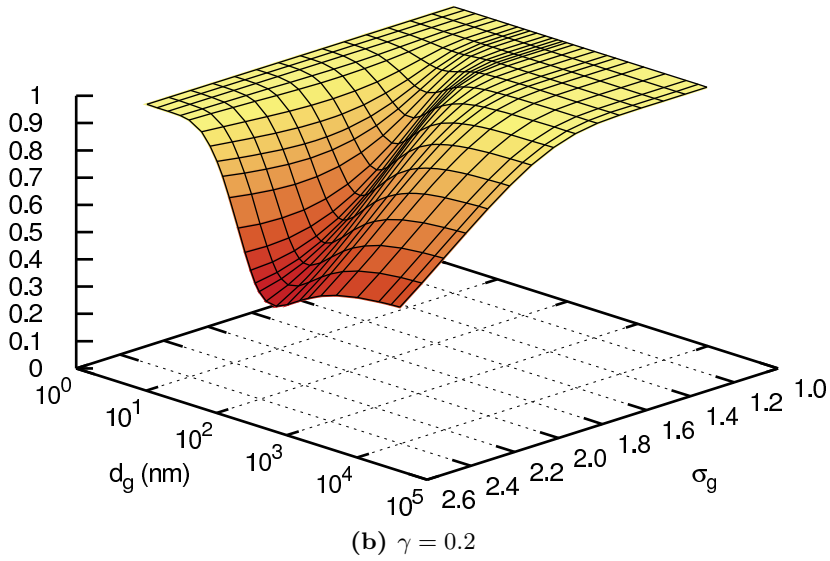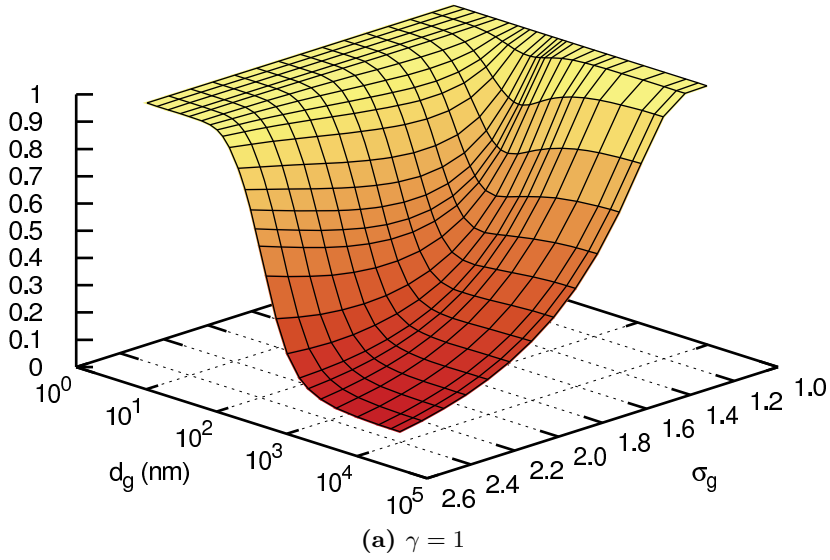
Figure 4: SA quality parameter ξ as a function of the PA parameters d_g and σ_g. Situations where aerosol is separated from the peak (a) and from the low mobility tail (b) of the PA distribution are shown.

exists in the d_g scale, after which the quality increases again, however, generally not reaching the previous maximum. This effect is especially visible on the second graph where it can be seen that this quality "valley" is located at around 200 nm. The reason for this "valley" originates from how differently charged components of PA overlap in the mobility scale which depends on the charging probabilities of particles (in Equation (10) n_i is a function of p_i) and thus on d_g.

To give an overview of SA quality in case of different values of the PA parameters d_g and σ_g, the required shifts γ towards the lower mobility end of the distribution of PA to obtain the quality of at least 95% and the available relative particle concentrations in those cases are presented in Table 1. As it can be seen, in some situations the 95% quality is unattainable with reasonable values of γ and n_N.

3.3 Discussion

As the relative amount of multiply charged particles in SA decreases when moving the separation point towards the lower mobility end of the PA (Figure 3), then, starting from a certain mobility, the concentration of doubly charged particles can be below some limit to be practically relevant/detectable (i.e. comparable in magnitude with the measurement error). However, this limit can be practically valid only for a certain instrument or setup – the fact that for a given instrument there appear to be no multiply charged particles does not mean that they are actually not present and detectable by another instrument. For some applications, accepting also low particle concentrations, such reasoning may be sufficient and the complicated calculations are not necessary. When generating standard aerosols for instrument calibration where larger particle sizes and higher concentrations are required, however, the situation is different and a guaranteed high-quality standard aerosol is required. Thus, a better method for producing the standard aerosols is necessary.

Table 1: The highest possible γ (the smallest required shift) to obtain $\xi \geq 0.95$ and corresponding values of n_N (%) $[\gamma; n_N]$ in case of different PA parameter d_g and σ_g values. Abbreviation n/a denotes the situation where $\gamma < 0.1$, i.e., for practical purposes the required ξ is unattainable.

σ_g	d_g (nm)					
	10	20	50	150	750	10000
1.2	1.00; 0.72%	1.00; 1.61%	1.00; 4.18%	1.00; 9.31%	1.00; 16.90%	1.00; 20.73%
1.5	1.00; 0.26%	1.00; 0.59%	0.18; 0.57%	0.23; 0.84%	0.31; 0.88%	0.31; 0.51%
1.8	1.00; 0.13%	1.00; 0.30%	n/a	n/a	0.15; 0.42%	0.18; 0.50%
2.1	1.00; 0.07%	1.00; 0.17%	n/a	n/a	n/a	n/a
2.4	1.00; 0.04%	1.00; 0.10%	n/a	n/a	n/a	n/a

4 Obtaining higher-quality standard aerosols

4.1 A method for avoiding the multiple charges problem

As shown above, problems arise when using the conventional methods for generating calibration aerosols – the presence of multiple charges on particles imposes limitations on the usability of the produced standard aerosol. However, a simple method exists which completely removes the effect of multiple charges and allows a much more efficient usage of the generated calibration aerosol. Instead of the conventional scheme where simply the particles of a required size range are produced and then charged or neutralized, a two-step process is used, as in the well-known LaMer generator (Sinclair & LaMer, 1949). During the first step, initial small particles (nuclei) are generated and then charged. As the particles are small, the probability of their acquiring more than one elementary charge is very low. Finally, these particles are grown to the required size. As a result, such primary aerosol contains particles with no more than a single charge and also has a much narrower size distribution of particles compared to the usual PA produced by one-step process (usually, by atomization of some solution with consecutive drying of droplets or by atomization of nonvolatile liquids). The calibration aerosol produced by this method is of higher quality. As there are no multiple charges, the whole width of the PA distribution can be used – there is no need to seek the "tail" as previously. This means that the peak of the distribution becomes available, giving much higher signal levels for calibration. However, care must be taken not to have a too high concentration of the initial nuclei.The reason seems to be that some of the charged nuclei may remain small (undeveloped) and act as charging ions, causing multiple charges on grown particles. Similar effect may also appear even with low concentrations of nuclei, if the particles are not well mixed in the growth chamber and some of the nuclei may pass through without a significant growth.

4.2 Experimental verification of the theoretical considerations

To test the new method for generating standard aerosols, a series of experiments was carried out [II]. The experiment setup is shown in Figure 5.

Silver particles (nuclei) were generated in a tube furnace. The obtained aerosol was diluted (see previous section) and then passed through a neutralizer and an ion trap (which removes the light charger ions). In a modified LaMer-type condensational generator (growth chamber) the charged particles are grown larger using DOP vapors. Finally, the grown charged
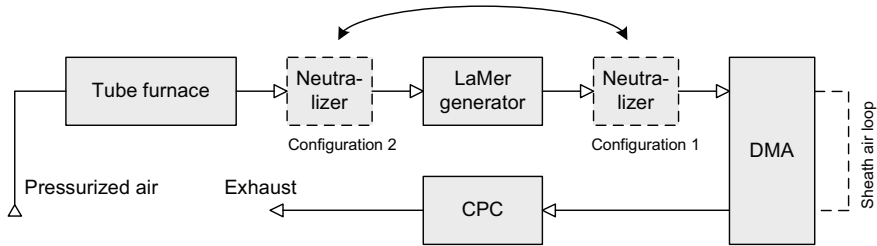
Figure 5: Block diagram of the experiment setup. The position of the neutralizer in different setups is indicated with a dashed line and an arrow. The diluter for the nuclei after the tube furnace and the ion trap before the LaMer generator are omitted for clarity.

particles were led to a Vienna design-based DMA and a CPC. For the separation of large particles ($d > 1\ \mu m$), the Very Long DMA (see section 5.1) was used.

The experiments were conducted using two different instrument setups. In the first (conventional) configuration, the neutralizer was placed after the growth chamber so that the already grown particles were charged. In the second (new) configuration, the charger (neutralizer) was connected before the growth chamber where the nuclei were charged before they were grown to a larger size (Figure 5). In both cases, at the alternative position for the neutralizer, a "dummy" device was used with the same construction as the real neutralizer only with the radioactive source absent. This was done in order to equalize diffusional and inertial particle losses in both setups.

The main idea behind the experiments is to verify that the aerosol obtained from the second setup (the new method) does, indeed, not contain any particles with multiple charges and thus has perfect quality. If this is the case, then it should be possible to theoretically find the expected particle mobility distribution of the first (conventional) setup using the measured particle distribution from the new setup, and match it with the actual measured distribution of the conventional setup. Otherwise, if the expectedly perfect quality aerosol contains a noticeable number of multiply charged particles, there should be a large difference between the calculated and measured distributions.

4.3   Description of the calculations

In the experiments, the nuclei were grown to the final size distribution with the mean diameter of approximately 1300 nm to ensure high charging probabilities in case of the conventional setup. The particles were charged in two different setups as described above and, using a DMA and CPC, the

number concentration of the charged particles (of one sign) at the DMA outlet as a function of the DMA transfer function midpoint mobility (DMA response) was determined in both cases.

For the calculations, first the mobility distribution density of PA must be found. The mobility distribution density $f(k)$ of the particle number concentration n (normed to the total number concentration) is defined as:

$$f(k) = \frac{\mathrm{d}n}{\mathrm{d}k} \,.$$

(11)

From here, the concentration as a function of the DMA transfer function midpoint mobility k' (i.e., the actually measured quantity – DMA response $n(k')$) is found as an integral over the product of the distribution density function and the DMA transfer function. As noted before, the DMA transfer function is considered triangular (Equation (4)) with only the DMA geometry and regime parameters determining its width. The distribution density function is taken as a constant in the narrow range between the DMA transfer function endpoints (limiting mobilities). Thus the DMA response $n(k')$ can be, instead of an integral, written as an area of a triangle:

$$n(k') = \frac{1}{2}f(k')2k'\beta \,,$$

(12)

where $2k'\beta$ is the width of the DMA transfer function (β is the relative half-width) and $f(k')$ is the mobility distribution density function. Finally, using Equation (12) and the mean charging probability for the nuclei p_m, the notional mobility distribution density function of *all* particles (as if they were all singly charged) $\phi^*(k') = f(k')/p_m$ is found from the experimentally measured $n(k')$ from the new setup:

$$\phi^*(k') = \frac{n(k')}{k'\beta p_m} \,.$$

(13)

For the charging probability p_m, the size distribution of the nuclei was also measured during the experiment and the probability corresponding to the peak of the size distribution was used. From this notional distribution density, the expected (theoretical) DMA responses $n_i(k')$ of i times charged particles were found using the corresponding charging probabilities p_i:

$$n_i(k') = \phi^*\left(\frac{k'}{i}\right) p_i \left(d\left(\frac{k'}{i}\right)\right) \beta\frac{k'}{i} \,.$$

(14)

Here $d(k'/i)$ is the apparent particle diameter, corresponding to the mobility k'/i. The arguments k' in Equation (14) are divided by the number

of charges i to shift the functions in the mobility scale, thus taking into account the fact that a particle with i charges has an electrical mobility i times greater than that of the equally sized particle with only one charge.

The total theoretical DMA response for the conventional setup was finally calculated as a sum of the theoretical response functions of the differently charged particle fractions. This was then compared to the actual DMA response obtained from the experiments with the conventional setup. If the aerosol from the new setup has a (near) perfect quality, then these two should match.

4.4 Experimental results

The DMA response obtained experimentally using the new setup is shown in Figure 6 (the curve with a single mode). It can be seen that despite the high particle size of around 1300 nm, there are no significant multiple charge fractions and the general shape of the function follows that of the lognormal curve ($R^2 = 0.996$). There is, however, a slight deviation from the lognormal function towards the higher mobilities for which an explanation is given below.

From the function in Figure 6, the theoretical (apparent) mobility distribution density of all particles (if they were all singly charged) was found (using Equation (13)). This enabled to model what would happen if the initial aerosol with this distribution density was charged in the conventional setup. The theoretical outcome is shown in Figure 7, where the functions corresponding to the differently charged fractions are described by Equation (14). The slight deviation from the lognormal function, as mentioned above, was small enough that an attempt to model it with a second lognormal function would not have given reliable results, thus the uncorrected lognormal fit was used.

In Figure 6 also the theoretical DMA response from the conventional setup is compared to the one determined experimentally. The model and the measurement data for the conventional setup are in a good general agreement. As expected and described by the model, the overall function consists of differently charged particle fractions (note the two small peaks visible in both the conventional setup data and the model DMA response at $k \approx 2 \times 10^{-9}$ m^2/Vs and $k \approx 3 \times 10^{-9}$ m^2/Vs). There is a small difference between the concentrations of the model and the experimental data from the conventional setup, which originates from different particle losses between the two setups (in different setups the same route is traveled by differently charged particles). The total concentration for the conventional setup is also much higher compared to the new setup. This is expected, as
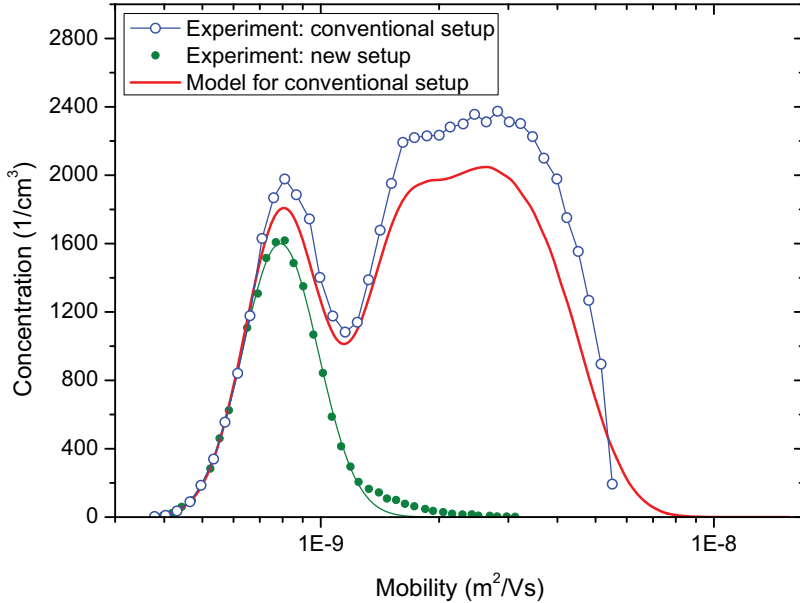
Figure 6: Measured DMA responses of PA particles from the conventional and the new setup and the model function for the conventional setup.

it comes from the nature of the new setup, where the charging probabilities are determined by the size of the nuclei not the final grown particles. In order to avoid any misunderstandings, a further note must be added. In Figure 7, the density functions of differently charged components are comparatively weakly overlapped, so that SA with a good quality seems to be achievable even when the separation point of particles is at the peak mobility of singly charged particles. It must be considered, however, that the components in Figure 7 are calculated for PA with $\sigma_g = 1.25$, and even here $\xi \approx 0.9$. With the conventional method, as a rule, PA with σ_g around 2 is used and ξ has a much lower value. The new setup guarantees here $\xi \approx 1$.

4.5   Discussion

As mentioned above, in Figure 6, a deviation of the measured data from the lognormal function can be seen. This is most likely caused by the presence of doubly charged particles, despite the measured data coming from
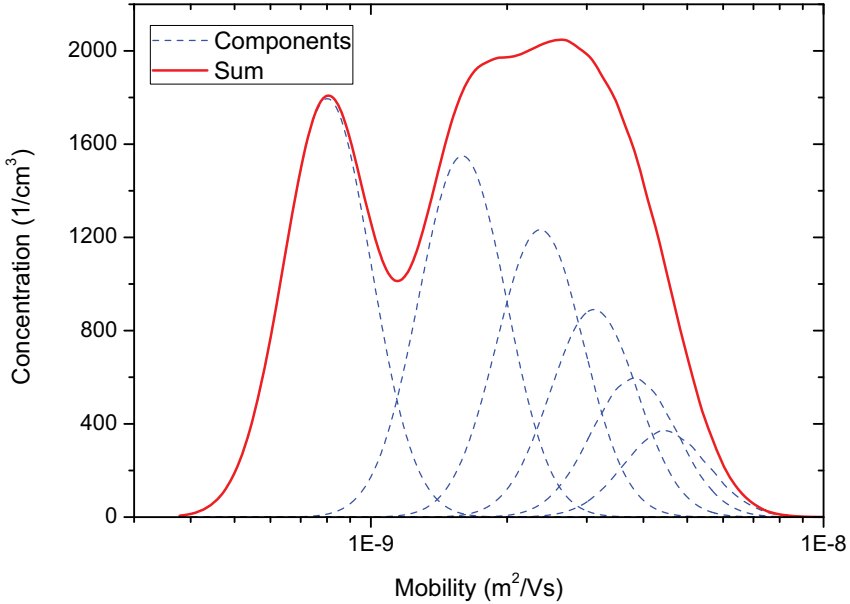
Figure 7: Model of the DMA response of PA particles describing the conventional method for producing aerosol. The differently charged fractions that make up the sum are also shown.

the new (improved) setup. The reason for their existence seems to be in the construction of the actual growth chamber used in the experiments. It seems that there is a region inside the generator where nuclei are not well mixed with the DOP vapor and can pass through without any significant growth. Some of the undeveloped charged nuclei can then coagulate with the grown charged particles (of the same sign) and thus also transfer their single charge. The evidence to support this comes from the fact that with the adding to the outlet of the generator of a turbulence-causing narrow nozzle which helps to mix the nuclei and the vapors, the amount of doubly charged particles is significantly reduced. This was observed in the experiments (particle diameter approximately 110 nm), where without the nozzle, a second peak was seen in the measured mobility distribution of the particles at the position of twice the mobility of the main peak. This peak of doubly charged particles constituted about 15% of the amount of all charged particles. With the addition of the nozzle, no second peak was seen. The effect, as seen in Figure 6 (with the presence of the nozzle being not

enough), was observed to disappear with smaller particles (the difference between the sizes of the nuclei and the larger particles is smaller, which gives a smaller coagulation coefficient) and with larger particles (higher generator temperature reduces the inhomogeneous area in the generator). Thus the effect does not arise from the shortcomings of the method in question, but from its actual implementation, i.e., a less efficient design of the generator. The influence of ungrown charged nuclei seems to be the only probable mechanism for producing multiple charges, as light ions cannot penetrate the ion trap before the LaMer generator (see the experiment setup) and the coagulation coefficient for particles of different sizes is much higher than that of the equal-sized particles.

It should be noted that the presence of doubly charged particles in this case does not affect the calculations in any significant way, as the amount of those particles is very low. When using this aerosol for instrument calibration, their influence is reduced even more, as it can be shown that when separating from the peak of the PA distribution, the number of multiply charged particles in the separated aerosol will be insignificantly small for this case.

Based on an analogous method to the one described above, an apparatus for realizing a standard for aerosol particle number concentration (single-charged aerosol reference – SCAR)) has been built and tested by Yli-Ojanperä et al. (2010), with references to this work.

5 High quality standard aerosols in a wide size range

As described previously, high quality standard aerosols can now be obtained in a wide size range, using electrical separation. To take an advantage of the presented method and produce particles in higher size ranges, a specially designed DMA is needed which is able to separate larger particles. Such an instrument – the Very Long DMA, was developed and built in 1980 at the Air Electricity Laboratory of the Tartu State University (now the Laboratory of Environmental Physics of the Institute of Physics of the University of Tartu) for the purposes of experimental calibration of the wide-range electrical aerosol spectrometer EAS (Mirme et al., 1981; Tammet, 1980, 1992; Tammet et al., 2002). A short description of this DMA as a separator of aerosol particles was first published in 1984 (Peil & Tamm, 1984). This DMA can principally separate particles with mean diameter of up to 10 µm, which is much higher than it is possible with other known long DMA-s (Hoppel, 1981; Seol et al., 2002; Myojo et al., 2004; Shimada et al., 2005).

5.1 The Very Long DMA

During the experimental work (see section 5.3), it was found that some additions or enhancements were needed in the DMA itself and in the overall measurement system. The main issue was the low particle concentrations at the DMA output, because of two factors: gravitational settling of large particles (e.g. 7.9 µm, as used in the experiments described below) in the inlet and outlet tracts of the DMA, and intrinsically rather low particle concentrations (for electrical separation method) of the polystyrene aerosols used. To combat this, first, the whole measurement system was reconfigured, so that all its components were positioned vertically relative to each other and with as short as possible connections between them. A new component, the virtual impactor (Marple & Chien, 1980; Chen & Yeh, 1987; Loo & Cork, 1988), was designed and built to boost the concentration of large particles. Also a new inlet section was designed and built for the Very Long DMA, minimizing the particle losses.

The technology of manufacturing the electrodes of the DMA could not ensure the ideal geometry of the DMA. Therefore, the real transfer function could be different from ideal. The Very Long DMA had been in use for years; however, no serious study of its performance was done during that time. In order to take a full advantage of the previously described method of obtaining high quality standard aerosols, the properties of the DMA used must be well known. Thus, an investigation of the performance of the Very
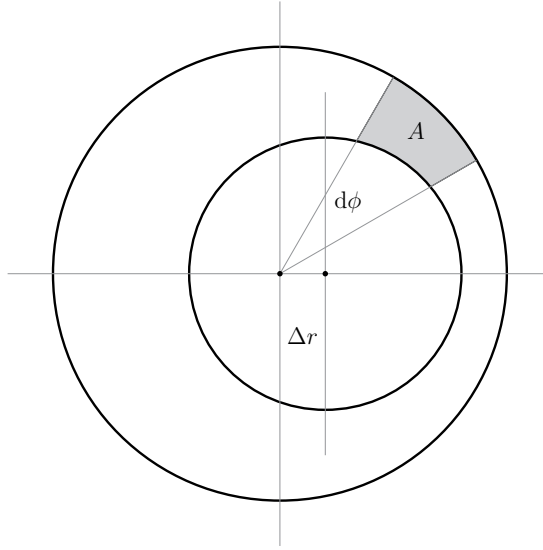
Figure 8: Cross-section of the cylindrical DMA electrodes. The outer electrode is divided into sectors with a central angle dϕ forming a vertical section (segment) between the electrodes with a cross section area A. The axes of the two cylinders are shifted by Δr.

Long DMA was done. This consisted of two main parts: the theoretical investigation of the possible effect of manufactoring non-idealities of the DMA on its transfer function and the experimental determination of the DMA transfer function.

5.2 Distortions of the DMA transfer function: theoretical investigation

In the theoretical investigation of the transfer function of the Very Long DMA the effect on non-concentric electrodes of the DMA was studied [III, VII]. An analytical approach to solve this problem was made by Knutson (1971). In this work a numerical method (realized in Matlab) was employed using a simple model of the Very Long DMA.

To calculate the DMA transfer function, the space between the electrodes was divided into 1000 vertical sections (segments) so that the cross section of the outer electrode (also the inner one, if they are concentric) was comprised of sectors with equal central angles dϕ (Figure 8). The overall transfer function was calculated as an average of transfer functions of these individual sections. The limiting mobilities and transfer functions were calculated according to Equations (1) and (4). This was possible be-
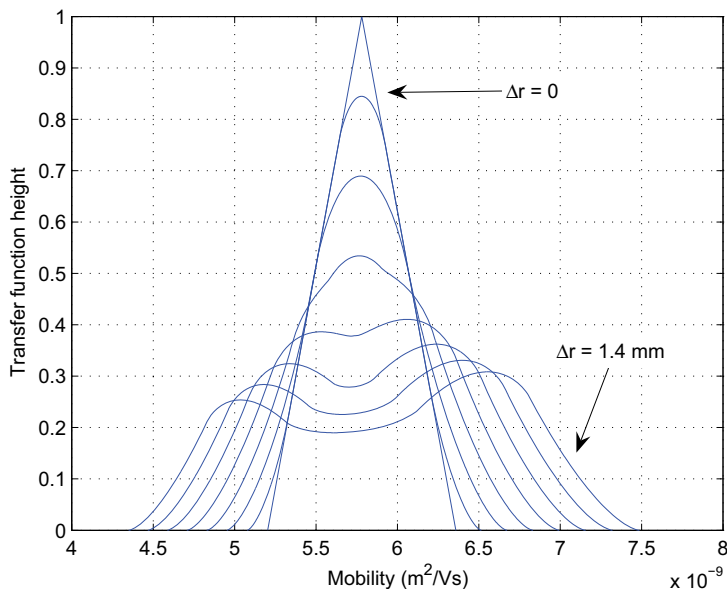
Figure 9: Theoretically found DMA transfer function in case of different distances $\Delta r = 0$, 0.2, ..., 1.4 mm between the axes of the cylindrical electrodes.

cause according to Tammet (1970), the general theory developed for the cylindrical aspiration capacitor is applicable to a sector of the cylindrical capacitor, as well as to the parallel-plate capacitor. The volume flow rates in the sections were taken to be proportional to the area A of its cross section, i.e. the profile of the air flow was considered to be uniform and not dependent on the distance between the electrodes (the model of the ideal fluid was used). A numerical flow simulation, using a 3D CAD model of the Very Long DMA, was also briefly used for finding the flow rates, but in the end, the simpler and computationally much cheaper method was chosen. For finding the capacitance of the section, the corresponding parts of the inner and outer electrode were taken to form a parallel-plate capacitor with the width of the plate being determined by the part of the inner electrode.

The results of the calculations, modelling the shift of the electrodes, are presented in Figure 9. As it can be seen, without the shift between the axes of the cylinders, the transfer function has the expected triangular shape. With increasing Δr, however, the transfer function gets wider and lower until actually several maxima appear. A significant decrease in the transfer function height can already be seen with shifts between the cylinder axes below 1 mm. Analogous distortions of the transfer function could also appear in the case of a slightly curved central electrode, which can exist

32

due to the production technology of the Very Long DMA (the electrodes of the DMA are not made from one long piece, instead, they are comprised of individual sections, glued together).

Theoretical assessment of the DMA transfer function was performed using the model of ideal fluid, i.e. the velocity profile between the cylindrical electrodes of the DMA was assumed uniform. Partial flow rates for imaginary vertical sectors of the space between the non-concentric cylindrical electrodes were assumed to differ from each other only due to different cross section areas of the sectors. In case of real (viscous) fluid, the difference in mean velocities and, therefore, also in partial flow rates between the sectors of different cross section areas is higher than in case of the ideal fluid model. Therefore, the general nature of distortions in the transfer function should be the same in both cases. The only difference should be in the magnitude, with the case of the real fluid having larger distortions.

5.3 Distortions of the DMA transfer function: experimental investigation

The theoretical results showed that considering the construction methods of the Very Long DMA, the distortions of its transfer function are likely to occur. Thus an experimental study, to determine the transfer function of the Very Long DMA, was done as well, to see whether any of the theoretically predicted effects would be observed.

For determining the transfer function of a DMA, usually some form of a tandem-DMA setup is used (Fissan et al., 1996; Stratmann et al., 1997; Birmili et al., 1997; Martinsson et al., 2001) [IV]. Here, however, this method is not suitable, as in addition to the DMA under investigation, it requires the presence of another, identical or at least similarly capable DMA. As the Very Long DMA is rather unique, this is not possible. Another way for determining the DMA transfer function, which does not require multiple DMAs, is to measure a highly monodisperse aerosol. From Equation (9) it can be seen that when scanning over the aerosol distribution with a DMA, the measurement result (particle number concentration on the output of the DMA) is a convolution between the aerosol distribution and the DMA transfer function. If the aerosol distribution is very narrow (much narrower than the DMA transfer function), then the measurement result can be approximated as a convolution between the transfer function and a delta function, which is equal to the transfer function itself. Although in the strict sense, this analogy is not perfect – when scanning over the narrow distribution, the absolute width of the DMA transfer function increases and thus the convolution does not yield a perfect representation of the original
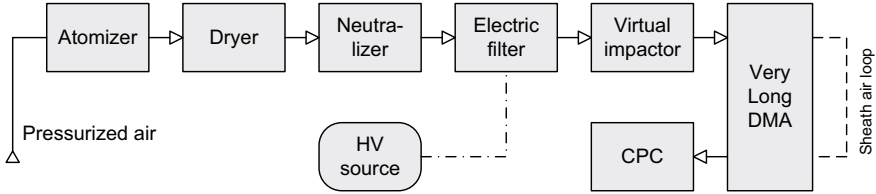
33

Figure 10: Experimental setup for determining the transfer function of the Very Long DMA.

transfer function, even with an ideal delta function as the input. However, calculations show that the error made in this way is insignificant, compared to the measurement errors and thus the approximation is usable.

Experimental setup is presented in Figure 10. A suspension of polystyrene microspheres with the mean diameter of 1 (0.994) µm and standard deviation of 0.010 µm was atomized to produce a monodisperse test aerosol. The obtained aerosol was first dried in a silica gel drier and neutralized using a ^{239}Pu neutralizer and then directed through an electric filter and a virtual impactor (see also section5.1).

The electric filter was designed and added to the system to suppress the electric wind that can arise inside the DMA and distort the DMA transfer function. The electric wind was known to be a factor that needed attention when using the Very Long DMA, however, usually the method that gives only singly charged particles (section 4) is used and the electric wind arises only with high voltages. Here, polystyrene aerosol is used that is produced of a suspension containing also a stabilizing agent, meant to prevent the coagulation of the polysterene spheres. Due to the rather low solid content of the atomized suspension, most of the generated droplets are "empty", containing stabilizer but no polystyrene sphere. After drying, the stabilizer forms small particles that obtain a stationary charge distribution in the neutralizer. The high charge density that comes from the large number of these small charged particles can cause the electric wind at already quite low voltages. Electric filter removes these small charged particles and prevents the electric wind from arising.

Finally, the dependence of the DMA output signal (particle number concentration) on the voltage on it was measured using the Very Long DMA and a CPC. A triangular function (Equation (4)) was fitted to the measured distribution of the output concentration for singly charged particles (due to the very high monodispersity of the polystyrene particles, singly and multiply charged particles in the measured distribution were easily distinguished, i.e. there was no overlapping) and the relative half-width β
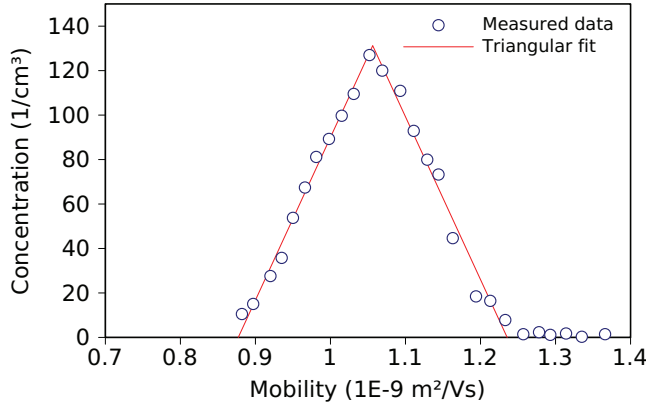
Figure 11: Experimentally found DMA transfer function.

of the function was obtained (Figure 11). Here, only the half-width of the transfer function was examined and the height (and area) of the transfer function were not investigated, as the total aerosol concentration is, in this case, practically impossible to determine. The measurement results gave β = 0.17 (ideal value, determined by the DMA airflows, would be 0.1). The difference between the experimentally found and ideal value ofβ suggests that there are some imperfections in the DMA construction. However, no significant distortions in the shape of the transfer function of the Very Long DMA were observed.

As stated previously, the height of the DMA transfer function was not investigated, therefore, the vertical axis in Figure 11 shows the aerosol concentration as measured by the CPC. This is presented to illustrate the relatively low particle concentrations available, which can make the described experiments difficult. Attempts were also made to use aerosols with 7.9 µm mean diameter, as the Very Long DMA is capable of measuring/separating particles with diameter up to 10 µm. However, while the solid content of the 7.9 µm suspension is approximately 10 times higher than that of the 1 µm suspension, the volume of a particle is 10^3 times higher, which gives much lower number concentrations and makes the particle detection/counting even more difficult. Also the model of the CPC used (TSI model 3776) has a measurement efficiency of about only 30% in this particle size range (Farnsworth & Caldow, 2011). It must be noted, though, that while performing the actual experiment with larger particles was impossible, yet, there are no strong arguments why the transfer function of the Very Long DMA should be different with larger particles. Only the gravitational shift of the transfer function of the DMA [V] must be considered.

6 Applications of the standard aerosol generation setup

The instrument setup for realizing the above-described method for producing high-quality standard aerosols has been used for the calibration of the Electrical Aerosol Spectrometers (EAS; see also the beginning of section 5) and Air Ion Spectrometers (in a reduced configuration) [V, IX, X]. For example, the work described in [V] was a part of a larger joint calibration campaign, where the Estonian part of the work was done using the calibration setup described below and managed by the author. The calibration system's full capability has also been recently employed in the calibration of a new version of the EAS, results of which (along with the description of the new EAS itself) have not yet been published. Parts of this calibration setup have been mentioned above; here, the full description is given.

The full setup is shown in Figure 12 (see also section 4.2). A polydisperse aerosol with silver particles in a size range from a few to about 40 nanometers is produced in a tube furnace. The aerosol is optionally diluted by directing some of the airflow from the furnace through a fiber filter. It is then charged in a bipolar charger and either directed to the DMA (in case of the calibration of ion spectrometers – reduced configuration), or diverted for further processing. From this diverted aerosol, first, any light ions from the charger are removed by the ion trap and then the aerosol is led to a modified LaMer generator (Sinclair & LaMer, 1949) where the aerosol particles grow to larger sizes. The aerosol with grown particles finally reaches the DMA. In the DMA the aerosol particles are separated according to their electrical mobility and the now monodisperse (standard) aerosol outputs to the mixing chamber.

The mixing chamber is a convenient way of performing the various tasks that are needed during calibration. It is mainly used as the outlet of the standard aerosol from the DMA (with some clean extra make-up air added), which is connected with the instrument that is being calibrated. Because of the multiple outputs of the mixing chamber, the standard aerosol can be at the same time monitored by another instrument, e.g., CPC, aerosol electrometer, DMA or some other, already calibrated aerosol spectrometer.

The DMA that is used for the separation of particles is chosen according to the desired particle size: up to around hundred nanometers, a small Vienna-type DMA is used (see also appendix B), for larger particles, the Very Long DMA, described in section 5, is employed.

In the system, tasks like setting the DMA voltage(s), measuring the various flowrates and collecting data from instruments, such as CPC or aerosol
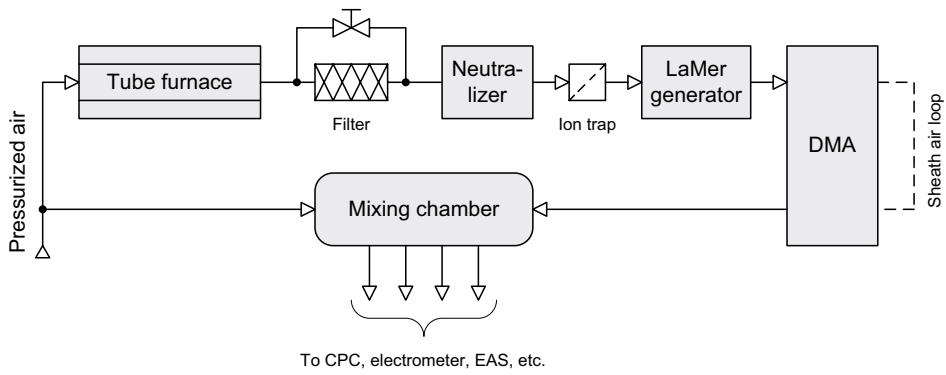
Figure 12: Schematic of the calibration setup. Not all parts of the setup are used at the same time, but are selected according to the particular system configuration.

electrometer, are handled by a personal computer, running a specifically written software package (Uin, 2005).

7 Conclusions

Highlights

The electrical separation method for producing standard aerosols for instrument calibration has been in use for some time. By nature, it is a rather versatile method, however, so far it has been limited for use with only rather small particle sizes, because of the multiple charge problem. Different tactics have been employed to diminish the effect of multiple charges. It was shown in section 3, that in reality, even with small particle sizes, the current schemes for the electrical separation do not always produce good results. Getting a high quality standard aerosol is not always a straightforward process and often a good understanding of the setup and initial aerosol is needed. A new method was proposed and characterized in section 4, that allows to obtain high-quality standard aerosols regardless of their particle size. Using this method with the Very Long DMA, investigated in section 5, has allowed to reliably calibrate various aerosol spectrometers in a wide particle size range.

Open problems

While the work presented above answered many questions, it also presented new ones. Some of the subjects explored need additional further study. Below is a list of the more important topics that need further attention.

1. The exact mechanism for the appearance of the low quality region described in section 3.2. It can easily be seen that its direct cause originates from how the charging probability functions for different numbers of charges behave in the particle diameter scale. However, more thorough theoretical work would be in order here.

2. Better experimental investigation of the standard aerosol quality. In the appendix A, two different attempts at the experimental determination of SA quality are detailed. Both give results that, in general, support the theory (an increase in quality together with the increasing particle size can be seen), but do not follow closely the exact numbers given by the theory. Instruments with higher capabilities than those available are needed for this work.

3. Better design of the modified LaMer generator. In section 4.5 it was described how the current design of this apparatus can cause multiply charged particles to appear in the SA. Currently, several possible design improvements are awaiting experimental verification.

4. Thorough investigation of the electric wind in the Very Long DMA. Currently, somewhat empirical knowledge is used when working with this instrument and a better understanding of this effect is needed. Also, the Very Long DMA has built-in features (special windows) meant for the visual observation of the aerosol layer(s) between the electrodes. A more usable electronic method (a kind of CCTV system) is planned so that the situation inside the DMA could be constantly observed.

5. Continuation of the attempts to determine experimentally the transfer function of the Very Long DMA for particle sizes above 1 µm. As it was described in section 5.3, the experiments with particle sizes around 8 micrometers did not yield results due to the very low particle number concentrations. Ways to decrease the particle losses inside the measurement system or the possibilities of using particle detectors with higher efficiency need further study.

6. Experimental investigation of the effect of gravity when separating particles in the 8 micrometer size range. Theoretical investigation (Bronec et al., 1999)[V] shows that the effect of gravity should shift the DMA transfer function. So far it has been impossible to observe this effect in reality due to the reasons outlined at the end of section 5.3.

Appendix A   About experimentally determining the SA quality

The results from calculations described in section 3.2 show that the decrease in standard aerosol quality with the increasing particle size is not monotonic. There is a region, a "valley", where the quality reaches its minimum and then starts to increase slightly again. This was a purely theoretical result and a question was raised whether this could also be examined experimentally. To this end, two separate sets of experiments were performed.

A.1   First method

Aerosols with $\sigma_g \approx 1.3$ and d_g in the range of $50 - 400$ nm, were produced using the setup described in section 4.2 with the charger *after* the LaMer generator ("configuration 1" in Figure 5) [VIII]. The charged particles were then separated with the Very Long DMA. As some of the particles were multiply charged, the separated aerosol consisted of differently charged particle size fractions with their mobilities in the same narrow interval.

Determining the SA quality requires that the concentrations of these charged fractions in SA (Equation (7)) were known. To accomplish this, the size distribution density of separated particles was measured with a TSI SMPS system consisting of a neutralizer, a Long DMA and a CPC. By using the SMPS's own neutralizer, each of the previously differently charged fractions obtained its own (near-) Boltzmann charge distribution (Figure 13). A multiple charge correction algorithm (by TSI software) was applied to the SMPS measurement data, resulting in a size distribution density with multiple modes corresponding to the previously differently charged fractions in SA. A sum of lognormal functions was fitted to the data and by integration, the concentrations of individual components were found. Finally, the quality of SA was calculated using these concentrations. The quality was found for different values of d_g (with $\sigma_g \approx 1.35$) and repeated several times.

A.2   Second method

Aerosol generation setup, identical to the one described in the previous section, was used to produce aerosols with σ_g in the range approximately from 1.28 to 1.32 (it was difficult to keep the σ_g constant) and d_g in the range of $100 - 300$ nm [I]. Again, as some of the particles were multiply charged, the separated aerosol consisted of differently charged particle size
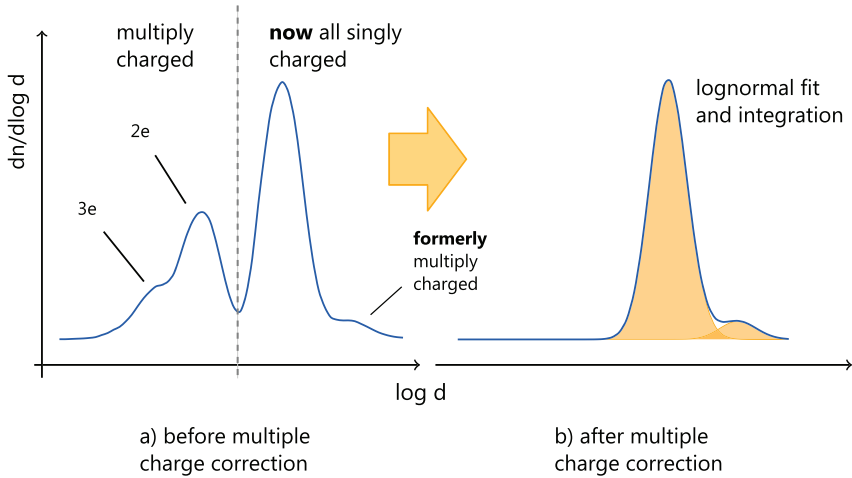
Figure 13: The application of a second neutralizer and a multiple charge correction algorithm for experimentally determining the SA quality.

fractions. The size distribution of the separated aerosol was then measured with an optical aerosol spectrometer (Micro Laser Particle Spectrometer manufactured by PMS), which clearly showed separate size fractions in the SA, corresponding to the differently charged particles. The particle number concentrations for these fractions were measured and the quality parameter was calculated using Equation (7). The experiment setup was then switched to the mode where only singly charged particles are produced (configuration 2 in Figure 5) and the d_g and σ_g of the primary aerosol (PA) size distribution were found by fitting a lognormal function to the experimental data. The theoretical quality parameter was calculated from these values and compared to the one obtained experimentally.

Possible measurement errors were estimated, with the main source of error judged to be in the determination of σ_g – standard deviation from the lognormal fit (essentially possible measurement uncertainty at 67% confidence level) was $\pm$ 0.02 on average which gives approximately $\pm$ 0.03 for the theoretically calculated ξ.

A.3   Results and discussion

Experimental results from the first method confirm the existence of the quality "valley" seen in the theoretical results presented in section 3.2; however, its location differs from the theoretical results (Figure 14). The reason for the "valley" originates from how differently charged components of PA overlap in the mobility scale which has a complex dependence on the
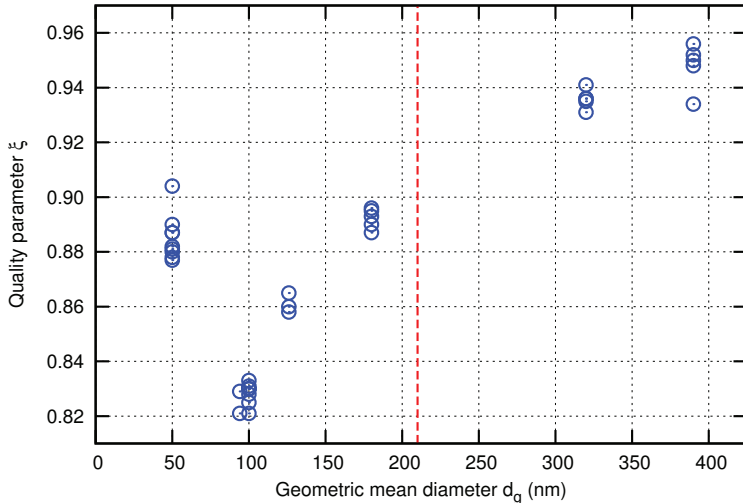
Figure 14: Results from the experiments for determining the SA quality using the TSI multiple charge correction algorithm. The vertical line shows the position of the theoretical quality "valley" in case of $\sigma_g = 1.35$.

charging probabilities of particles and thus on d_g. Such origin of the effect suggests that the theoretical calculations should be trusted and that the experimental results do not represent the actual position of the "valley" correctly. This could be caused by an asymmetric transfer function of the first DMA; however, calculations showed that this effect is relatively weak. Second, a more likely possibility is that in this complicated situation the multiple charge correction algorithm does not work very well and there are misestimations that change with the particle size.

Results of the second method show a general agreement between the experimentally found and theoretical quality (Table 2). However, the in-

Table 2: Experimentally found SA quality and the corresponding calculated quality in case of the experimentally found d_g and σ_g values. Estimated measurement errors for σ_g and ξ are given in parentheses.

d_g(nm)	$\sigma_g(\pm\ 0.02)$	exp. ξ	theor. $\xi\ (\pm\ 0.03)$
156	1.29	0.86	0.83
285	1.29	0.86	0.85
138	1.31	0.81	0.81
199	1.31	0.86	0.80
363	1.31	0.90	0.83

creasing trend of ξ in the d_g scale, found in the theoretical results, is very weak and (considering also the measurement uncertainties) difficult to find experimentally. In addition, the relatively low size resolution (in the higher diameter range) of the used optical spectrometer did not permit to use reliably the particle sizes over ~ 375 nm, i.e., to use data points at a higher d_g where theoretically the quality should also be higher, giving the greatest possible (and more easily detectable) difference in ξ as compared to the bottom of the theoretical "valley".

The existence of the theoretically found low-quality region remains unconfirmed in a strict sense due to the insufficient accuracy of the used instruments. However, there is evidence in favor of it as the experimental results do not show a monotonic decrease in SA quality with increasing particle size, which would be the case if the theoretically predicted low quality region was not present.

Appendix B Experimentally determined DMA transfer functions of "small" DMA-s

Most of the work presented in this thesis deals with the separation of large particles (diameters starting from a hundred nanometers) and the instrument used – the Very Long DMA. However, at times it became necessary to compare some aspects of its performance with those of another instrument. In addition to the work presented in section 5.2, the Very Long DMA was compared also to instruments that work in lower particle size ranges. In order to be confident in the obtained results, the performance of these instruments themselves needed to be well understood. Thus, the transfer functions of these instruments were determined as well.

Three different types of DMAs were investigated [IV]: a self-built Vienna-type DMA with modified aerosol and sheath air inlets and two TSI DMAs: a nano-DMA (model 3085) (Chen et al., 1996) and a Long-DMA (model 3081). The TSI DMAs were used as a part of the TSI SMPS system which also included the TSI model 3025A CPC and model 3080 Electrostatic Classifier. Silver or silver + DOP particles (the scheme described in section 4) (for particle diameters above 40 nm) were used for the experiments; particle concentrations were measured with the above-mentioned CPC. Experiments were controlled by a personal computer running a custom software package (Uin, 2005), which was responsible for setting the DMA voltages and collecting the data from CPC and air flow measurements. For the experiments, a standard tandem-DMA setup was used where two DMAs were connected in series. During each measurement the voltage applied to the first DMA was fixed at a value corresponding to the particle mobility/radius of interest, while the voltage of the second DMA was varied so that the mobility interval around the midpoint mobility of DMA1 was scanned. First, two identical Vienna-based DMAs were connected together and their transfer functions were determined as described by Stratmann et al. (1997), for particle radiuses in the range of 1.5 – 50 nm. Care was taken to assure that the two DMAs were identical – equality of the geometric dimensions of the two devices was carefully checked and several additional experiments were conducted where the outlet aerosol distributions of both devices were measured with a third DMA. Then TSI nano-DMA was paired with a previously investigated Vienna-based DMA and its transfer function was also determined.

Collected scan data were first normalized to the total aerosol concentration downstream of the DMA1, which was measured before and after every experiment by connecting the output of the DMA1 to the CPC in-
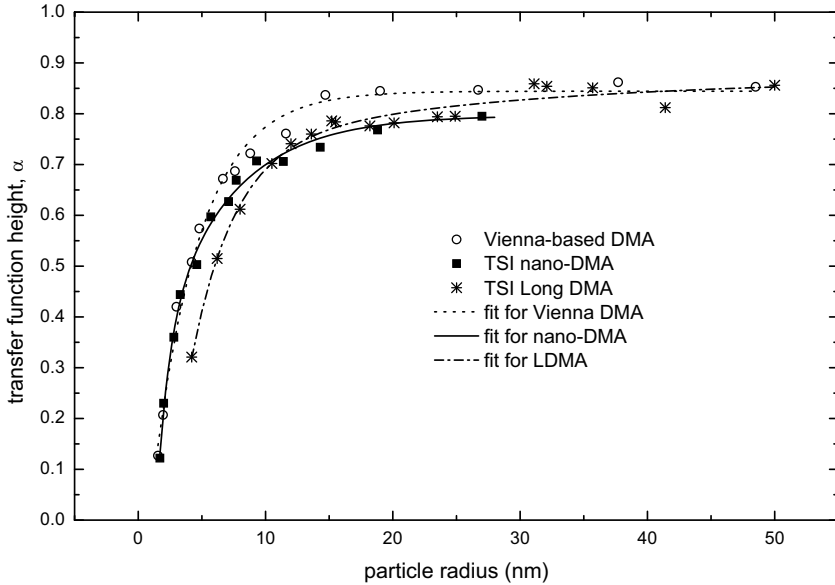
Figure 15: Dependence of the DMA transfer function height α on the particle size (radius) for the three different DMAs.

put. Effort was made to ensure that particle losses in the lines connecting the DMA1 to the DMA2 and in bypass lines to the CPC were the same, so that they would be canceled out by the normalization.Scan data were then deconvoluted using a simple iterative algorithm and assuming a triangular shape for the transfer function. The deconvolution algorithm uses a least-squares method to fit a theoretical mobility distribution at the output of the DMA2 to measurement data by varying the two transfer function parameters – the height α of the triangle and its relative half-width β at the given mobility. The values producing the closest fit are then taken as the actual values for the transfer function parameters at the current midpoint mobility of the DMA1, i.e., the particle radius of interest. In case of the nano-DMA and the Long-DMA, the calculations also require the values of α and β at the given particle radius for the previously investigated Vienna DMA. Because the data points (particle radiuses used) were not the same for both of the DMAs, the required transfer function parameter values were thus calculated from the function fitted to the α and β size-dependence data for the Vienna DMA.

Results show that all types of DMA-s have similar particle losses (value of α) for particle radiuses below 5 nm (Figure 15), but for larger particles
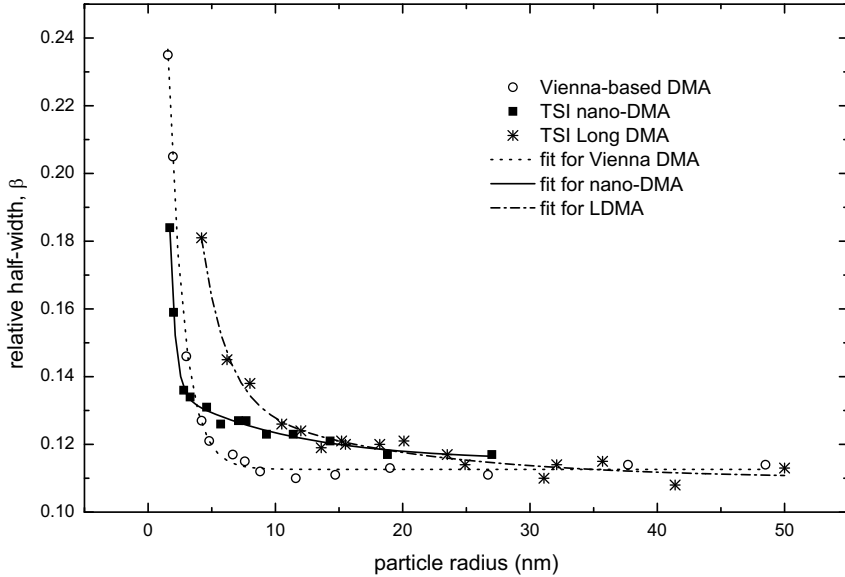
Figure 16: Dependence of the DMA transfer function relative half-width β on the particle size (radius) for the three different DMAs.

the losses are about 10% higher in case of the TSI nano-DMA. The particle transmission efficiency for the Vienna-based DMA levels off around 0.85 while that of the TSI Long-DMA keeps slightly increasing. For the transfer function relative half-width (DMA resolution) β, the Vienna-based DMA again has the best performance of the three, in case of particles with radiuses above ∼5 nm (Figure 16). The maximum difference is about 9% and goes down to 5% for larger particles. For the Vienna-based DMA, β levels off around 0.11 – close to the theoretical value of 0.1, determined by the DMA flowrates. For smaller particles, however, the situation is different – below ∼5 nm the nano-DMA has a significantly lower relative half-width compared to the Vienna DMA; the difference in β is as high as 30%.

Comparing these results with previous investigations of the TSI nano-DMA (Hummes et al., 1996; Chen et al., 1998), it can be seen that the results are in a general agreement for the relative half-width – the difference remains below 10%, with β having higher values (lower DMA resolution) in this work. The experimental results for the TSI Long-DMA also fit well with the previous results by Birmili et al. (1997) (taking into account the different flow rates and thus different theoretical β), no significant differences can be seen. For the transfer function height, the results for both of

the TSI DMAs seem to be constantly 10-15% lower (meaning higher particle losses) in this work for all investigated particle sizes. This indicates at the possibility that in the experiment setup, the particle losses between the DMA1-DMA2 and the DMA1-CPC might not have been as similar as intended.

Appendix C   Calculations and numerical modelling

The following sections describe the algorithms and numerical methods used for the calculations in the work presented above.

C.1   Quality calculation for bipolar aerosol

The following is a description of the procedure for performing the calculations described in section 3.1, presented in pseudocode. Original was written in Python, using NumPy.

1. Read in the chosen input parameters: γ and an array of $[\alpha,\ \beta,\ d_g,\ \sigma_g]$

2. For each element in array do:

    1. Calculate modal diameter d_m from d_g and σ_g
    2. Calculate the mobility corresponding to d_m and multiply it with γ to get k'
    3. Calculate n_i/N (Equation (10)) for $i = 1 \dots 6$:
        1. Calculate k_2 and k_3 using α, β and k'
        2. Calculate the integrating limits in diameter scale $d(k_2)$ and $d(k_3)$
        3. Do numerical integration to get n_i/N
    4. Calculate n/N as $\sum_i (n_i/N)$
    5. Calculate $\xi(n_1/N,\ n/N)$

C.2   Theoretical DMA response calculation for PA with multiply charged particles

The following is a description of the procedure for performing the analysis described in section 4.3. Original calculations were done using Mathcad and Origin.

1. Read in the experiment data from the new setup (only singly charged particles): array of $[k,\ I_E]$, where I_E is the current caused by charged particles, as measured by an aerosol electrometer.

2. Fit a lognormal function to the array of values $[k,\ I_E]$.

3. Calculate the distribution density (Equation (13)) using β and p_m (corresponding to the peak of the experimentally found size distribution of the nuclei).

4. Make copies of the distribution density function, corresponding to the particles with 1...6 charges. Shift them in mobility scale accordingly.

5. Convert the distribution density functions back to the distributions in the form of $I_E(k)$, accounting for different charging probabilities of particles with 1...6 charges.

6. Add the distributions of differently charged particles together (Figure 7 on page 28).

Nomenclature

α	height of the DMA transfer function
β	relative half-width of the DMA transfer function
γ	shift parameter, specifying the point of separation of particles
Φ	aerosol/air volume flow rate
ϕ^*	notional mobility distribution density function of all particles
σ_g	geometric standard deviation of PA size distribution function
φ	mobility distribution density of SA
d_g	particle geometric mean diameter of the PA
d_m	particle modal diameter of the PA
f	distribution (density) function of the PA
f^i	PA distribution (density) function of particles with i charges
H	DMA transfer function
i	number of elementary charges (of one sign) on particles
I_E	electrical current, measured by an aerosol electrometer
k	electrical mobility of a charged particle
k'	midpoint mobility of the DMA transfer function
k_1, k_2, k_3, k_4	limiting mobilities of the DMA transfer function
N	total number concentration of the particles of the PA
n	total number concentration of all charged particles of the SA
n_N	total number concentration of all charged particles of the SA, normalized to N
n_1	number concentration of SA particles with single charge
n_i	number concentration of SA particles with i charges
p_i	charging probability for particles with i charges
p_m	charging probability for the nuclei
PA	primary aerosol
SA	secondary aerosol

References

Berglund, R. & Liu, I. (1973). Generation of monodisperse aerosol standards. *Environ. Sci. Technol.*, 7, 147–153.

Birmili, W., F. Stratmann, Wiedensohler, A., Covert, D., Russell, L. M., & Berg, O. (1997). Determination of differential mobility analyzer transfer functions using identical instruments in series. *Aerosol Science and Technology*, 27, 215–223.

Bronec, E. L., Renoux, A., Boulaud, D., & Pourprix, M. (1999). Effect of gravity in differential mobility analysers. a new method to determine the density and mass of aerosol particles. *Journal of Aerosol Science*, 30(1), 89–103.

Chen, B. & Yeh, H. (1987). An improved virtual impactor: Design and performance. *Journal of Aerosol Science*, 18(2), 203–214.

Chen, D. & Pui, D. J. H. (1997). Numerical modeling of the performance of differential mobility analysers for nanometer aerosol measurements. *Journal of Aerosol Science*, 28, 985–1004.

Chen, D., Pui, D. Y. H., Hummes, D., Fissan, H., Quant, F. R., & Sem, G. J. (1996). Nanometer differential mobility analyzer (Nano-DMA): Design and numerical modeling. *Journal of Aerosol Science*, 27, S137–S138.

Chen, D. R., Pui, D. Y. H., Hummes, D., Fissan, H., Quant, F. R., & Sem, G. J. (1998). Design and evaluation of a nanometer aerosol differential mobility analyzer (Nano-DMA). *Journal of Aerosol Science*, 29, 497–509.

Farnsworth, J. E. & Caldow, R. (2011). A method for empirical measurement of cpc upper-end counting efficiency. In *International Aerosol Conference IAC2011, Helsinki*.

Fissan, H., Hummes, D., F. Stratmann, Büscher, P., Neumann, S., Pui, D., & Chen, D. (1996). Experimental comparison of four differential mobility analyzers for nanometer aerosol measurements. *Aerosol Science and Technology*, 24, 1–13.

Fuchs, N. A. (1947). On the magnitude of electrical charges carried by the particles of atmospheric aerocolloids. *Izvestiya Acad. Sci. USSR*, ser. geogr. geophys. 11, 341–348. in Russian with English abstract.

Fuchs, N. A. (1963). On the stationary charge distribution on aerosol particles in a bipolar ionic atmosphere. *Geofisica Pura e Applicata*, 56, 185–193.

Fuchs, N. A. (1964). *The Mechanics of Aerosols*. Pergamon Press.

Gupta, A. & McMurry, P. H. (1989). A device for generating singly charged particles in the 0.1-1.0 um diameter range. *Aerosol Science and Technology*, 10(3), 451.

Han, B., Shimada, M., Okuyama, K., & Choi, M. (2003). Classification of monodisperse aerosol particles using an adjustable soft x-ray charger. *Powder Technology*, 135-136, 336–344.

Hewitt, G. S. (1957). The charging of small particles for electrostatic precipitation. *AIEE Trans.*, 76(31), 300–306.

Hinds, W. C. (1999). *Aerosol Technology (Second Edition)*. John Wiley & Sons.

Hoppel, W. A. (1978). Determination of the aerosol size distribution from the mobility distribution of the charged fraction of aerosols. *Journal of Aerosol Science*, 9, 41–54.

Hoppel, W. A. (1981). Measurement of the aerosol size distribution with NRL's mobility analyzer. *Journal de Recherches Atmospheriques*, 15, 313–319.

Hõrrak, U., Mirme, A., Salm, J., Tamm, E., & Tammet, H. (1998). Air ion measurements as a source of information about atmospheric aerosols. *Atmospheric Research*, 46(3-4), 233–242.

Hummes, D., Neumann, S., Fissan, H., Chen, D. R., Pui, D. Y. H., Quant, F. R., & Sem, G. J. (1996). Nanometer differential mobility analyzer (Nano-DMA): Experimental evaluation and performance verification. *Journal of Aerosol Science*, 27, S135–S136.

Kikas, Ü., Susi, R., & Tamm, E. (1982). On the theory of the electrostatic separation of aerosols. *Acta et Comm. Univ. Tartuensis*, 631, 76–84. In Russian, summary in English.

Knutson, E. (1971). *The distribution of electric charge among the particles of an artificially charged aerosol*. PhD thesis, University of Minnesota.

Knutson, E. O. & Whitby, K. T. (1975). Aerosol classification by electric mobility: apparatus, theory, and applications. *Journal of Aerosol Science*, 6, 443–451.

Liu, B. Y. H. & Pui, D. Y. H. (1974). A submicron aerosol standard and the primary, absolute calibration of the condensation nuclei counter. *Journal of Colloid and Interface Science*, 47(1), 155–171.

Loo, B. W. & Cork, C. P. (1988). Development of high efficiency virtual impactors. *Aerosol Science and Technology*, 9(3), 167–176.

Mamakos, A., Ntziachristos, L., & Samaras, Z. (2007). Diffusion broadening of DMA transfer functions. numerical validation of stolzenburg model. *Journal of Aerosol Science*, 38(7), 747–763.

Marple, V. A. & Chien, C. M. (1980). Virtual impactors: a theoretical study. *Environmental Science and Technology*, 14(8), 976–985.

Martinsson, B. G., Karlsson, M. N. A., & Frank, G. (2001). Methodology to estimate the transfer function of individual differential mobility analyzers. *Aerosol Science and Technology*, 35, 815–823.

Mirme, A., Tamm, E., & Tammet, H. (1981). An aerosol electrogranulometer with a wide measurement range. *Acta et Comm. Univ. Tartuensis*, 588, 84–92. In Russian, summary in English.

Myojo, T., Ehara, K., Koyama, H., & Okuyama, K. (2004). Size measurement of polystyrene latex particles larger than 1 micrometer using a long differential mobility analyzer. *Aerosol Science and Technology*, 38(12), 1178–1184.

Peil, I. & Tamm, E. (1984). Generation of monodisperse aerosols by the electrostatic separation method. *Acta et Comm. Univ. Tartuensis*, 669, 44–52. In Russian, summary in English.

Peil, I., Tamm, E., & Zubchenko, P. (1992). Generation of a narrow bipolar charge distribution on aerosol particles. *Acta et. Comm. Univ. Tartuensis*, 947, 72–79.

Raabe, O. (1968). The dilution of monodisperse suspensions for aerosolisation. *Am. Ind. Hyg. Assoc. J.*, 29, 439–443.

Reischl, G. P. (1991). The relationship of input and output aerosol characteristics for an ideal differential mobility analyser particle standard. *Journal of Aerosol Science*, 22(3), 297–312.

Romay-Novas, F. J., . P. D. Y. H. (1988). Generation of monodisperse aerosols in the 0.1-1.0 um diameter range using a mobility classification-inertial impaction technique. *Aerosol Science and Technology*, 9, 123–131.

Seol, K. S., Yabumoto, J., & Takeuchi, K. (2002). A differential mobility analyzer with adjustable column length for wide particle-size-range measurements. *Journal of Aerosol Science*, 33(11), 1481–1492.

Shimada, M., Lee, H. M., Kim, C. S., Koyama, H., & Myojo, T. (2005). Development of an LDMA-FCE system for the measurement of submicron aerosol particles. *Journal of Chemical Engineering of Japan*, 38(1), 34–44.

Sinclair, D. & LaMer, V. K. (1949). Light scattering as a measure of particle size in aerosols. *Chemical Reviews*, 44(2), 245–267.

Stolzenburg, M. R. (1988). *An Ultrafine Aerosol Size Distribution Measuring System*. PhD thesis, University of Minnesota.

Stolzenburg, M. R. & McMurry, P. H. (2008). Equations governing single and tandem DMA - configurations and a new lognormal approximation to the transfer function. *Aerosol Science and Technology*, 42(6), 421–432.

Stratmann, F., Kauffeldt, T., Hummes, D., & Fissan, H. (1997). Differential electrical mobility analysis: A theoretical study. *Aerosol Science and Technology*, 26, 368–383.

Tamm, E. (1992). Electrical classification as a basis of the aerosol standard. *Journal of Aerosol Science*, 23 S1, S285–S288.

Tammet, H. (1970). *The aspiration method for the determination of atmospheric-ion spectra*. Jerusalem: Israel Program for Scientific Translations Ltd.

Tammet, H. (1980). On the techniques of aerosol electrical granulometry. *Acta et Comm. Univ. Tartuensis*, 534, 55–77. In Russian, summary in English.

Tammet, H. (1991). Aerosol electrical density: interpretation and principles of measurement. *Report Series in Aerosol Science*, 19, 128–133.

Tammet, H. (1992). On the techniques of aerosol electrical granulometry. *Acta et Comm. Univ. Tartuensis*, 947, 94–115.

Tammet, H., Mirme, A., & Tamm, E. (2002). Electrical aerosol spectrometer of Tartu University. *Atmospheric Research*, 62(3-4), 315–324.

Ude, S. & Fernandez de la Mora, J. (2005). Molecular monodisperse mobility and mass standards from electrosprays of tetra-alkyl ammonium halides. *Journal of Aerosol Science*, 36, 1224–1237.

Uin, J. (2005). Determination of the transfer function of a differential mobility analyzer in a dual aerosol analyzer experiment. Master's thesis, University of Tartu. In Estonian, summary in English.

Willeke, K. & Baron, P. A., Eds. (1993). *Aerosol Measurement. Principles, Techniques, and Applications*. Van Nostrand Reinhold.

Yli-Ojanperä, J., Mäkelä, J. M., Marjamäki, M., Rostedt, A., & Keskinen, J. (2010). Towards traceable particle number concentration standard: Single charged aerosol reference (SCAR). *Journal of Aerosol Science*, 41(8), 719–728.

Summary in Estonian

Elektriline separeerimine standardaerosoolide genereerimiseks osakeste suuruse laias vahemikus.

Käesoleva töö teemaks on aerosooliosakeste elektriline separeerimine kui meetod standardaerosoolide genereerimiseks. Erinevaid viise standardaersoolide tekitamiseks on mitmeid, kuid enamusel neist on mitmeseugused puudused ning enamasti on iga konkreetne meetod rakendatav ainult aerosooliosakeste kindlas suurustevahemikus. Üks universaalsemaid meetodeid nende hulgas on polüdisperssest aerosoolist monodispersse fraktsiooni eraldamine osakeste elektrilise liikuvuse järgi. Põhiprobleemiks antud meetodi juures on asjaolu, et osakeste elektriline liikuvus, mille järgi separeerimine toimub, on osakeste suurusega üheses seoses ainult siis, kui kõigil elektriliselt laetud osakestel on võrdsed laengud. Väikeste osakeste juures on bipolaarse laadumise korral see nõue täidetud – kõigil laetud osakestel on üks elementaarlaeng; suuremate diameetrite puhul tõuseb tõenäosus, et aerosooliosakene omandab laadimise käigus rohkem kui ühe elementaarlaengu. Tekib olukord, kus kordselt laetud suurel osakesel võib olla sama elektriline liikuvus, mis ühe elementaarlaenguga väikesel osakesel – kitsa liikuvusjaotusega separeeritud aerosool ei pruugi enam olla kitsa suurusjaotusega.

Antud efekti kirjeldamiseks tuuakse käesoleva töö osas 3 sisse separeeritud aerosooli kvaliteedi mõiste, mis kirjeldab kordselt laetud osakeste hulka separeeritud aerosoolis ja seega ka antud aerosooli "sobivust" kalibratsiooniaerosooliks. Lisaks on esitatud arvutuskäik standardaerosooli kvaliteedi leidmiseks, sõltuvana separeerimata (primaaraerosooli) jaotuse parameetritest. Antud arvutuste tulemused näitavad, et hetkel enimkasutatavad meetodid standardaerosooli saamiseks elektrilise separeerimise teel ei anna alati piisavalt hea kvaliteediga kalibratsioonaerosooli; tarvis on paremat meetodit.

Osas 4 on kirjeldatud ühte sellist meetodit, mis võimaldab genereerida standardaerosooli sõltumata osakeste suurusest. Antud meetodi põhiidee seisneb kaheastmelise osakeste tekitamise skeemi kasutamises, kus esmalt genereeritakse väikseid osakesi, mis seejärel laetakse ning kasvatatakse lõpuks nõutava lõpliku suuruseni. Kuna osakeste laadumistõenäosus on antud olukorras määratud esmaste, väikeste osakeste suurusega, siis lõplikud suured osakesed on samuti nõrgalt laetud. Toodud on antud meetodi detailne kirjeldus ning ülevaade eksperimentaalsest tööst, mille tulemused kinnitavad, et antud meetod tõepoolest võimaldab saada kõrge kvaliteediga standardaerooli.

Osas 5 kirjeldatakse unikaalset aerosooliosakeste elektrilist separaatorit, mis võimaldab eelkirjeldatud meetodit laias osakeste suurusvahemikus

rakendada. On toodud seadme lühikirjeldus ning lähemalt on kirjeldatud teoreetilist ja eksperimentaalset tööd antud instrumendi omaduste analüüsimiseks. Teoreetiliselt uuriti separaatori ehitusmeetoditest tuleneda võivaid mõjusid selle ülekandefunktsioonile, täpsemalt elektroodide kõverusest tuleneda võivaid efekte. Töö tulemused näitavad, et olulisi kõrvalekaldeid normist ei ole. Teiseks, määrati separaatori ülekandefunktsioon eksperimentaalselt, kasutades selleks uudset meetodit, mille põhisisuks oli monodispersse lateks-aerosooli liikuvusjaotuse mõõtmine. Saadud tulemused näitavad, et käesolev instrument töötab oodatud piirides.

Lõpuks on osas 6 lühidalt kirjeldatud, kuidas ülalesitatud meetodit ja seadmeid on kasutatud praktikas instrumentide kalibreerimiseks.

Käesoleva töö lisades on esitatud täiendava eksperimentaalse töö tulemused. Lisa A kirjeldab standardaerosooli kvaliteedi eksperimentaalseks määramiseks tehtud tööd ning selle tulemusi, mis üldjoontes toetavad osas 3 saadud teoreetilisi tulemusi. Töö põhieesmärgiks siin oli eksperimentaalselt leida kinnitust nn. kvaliteedi "lohu" olemasolule (vt. joonis 4). Leiti, et teatud suuruste piirkonnas separeeritud aerosooli kvaliteet tõepoolest tõuseb osakeste diameetri kasvades. Lisa B kirjeldab "väikeste" separaatorite ülekandefunktsioonide eksperimentaalset uurimist ning selle tulemusi. Ning lisas C on esitatud osades 3 ja 4 kirjeldatud arvutuste käik pseudokoodina.

Käesoleva töö käigus saadud tulemused võimaldavad senisest usaldusväärsemalt läbi viia erinevate aerosooliinstrumentide kalibratsiooni.

Acknowledgements

The author would like to express his gratitude to...

- supervisors Eduard Tamm and Aadu Mirme for their guidance and patience

- people at the Laboratory of Environmental Physics for all their help during these years

- language corrector Marika Liivamägi for her help in preparing many of my manuscripts (including this one)

- and last but not least, to my family for all their support.

Publications

Curriculum Vitae

General information

Name:	Janek Uin
Date and place of birth:	02.09.1980, Tartu, Estonia
Citizenship:	Estonian
Address:	Ülikooli 18, 50090, Tartu, Estonia
Phone:	+372 55 91 93 90
e-mail:	janek.uin@ut.ee

Education

1987 – 1996	Tartu Veeriku School
1996 – 1999	Tartu Mart Reiniku Gümnaasium
1999 – 2003	University of Tartu, Department of Physics, BSc, applied physics
2003 – 2005	University of Tartu, Department of Physics, MSc, applied physics
2005 – 2011	University of Tartu, Institute of Physics, PhD student

Employment

2005 – 2009	University of Tartu, Institute of Physics, engineer
2009 – ...	University of Tartu, Institute of Physics, specialist

Scientific work

Research and development of the instruments and methods for the calibration of aerosol instrumentation.

Curriculum Vitae

Üldinfo

Nimi:	Janek Uin
Sünniaeg ja -koht:	02.09.1980, Tartu, Eesti
Kodakondsus:	Eesti
Aadress:	Ülikooli 18, 50090, Tartu, Eesti
Telefon:	+372 55 91 93 90
e-post:	janek.uin@ut.ee

Haridus

1987 – 1996	Tartu Veeriku Kool
1996 – 1999	Tartu Mart Reiniku Gümnaasium
1999 – 2003	Tartu Ülikool, Füüsikaosakond, BSc, rakendusfüüsika
2003 – 2005	Tartu Ülikool, Füüsikaosakond, MSc, rakendusfüüsika
2005 – 2011	Tartu Ülikool, Füüsika Instituut, doktorant

Teenistuskäik

2005 – 2009	Tartu Ülikool, Füüsika Instituut, insener
2009 – ...	Tartu Ülikool, Füüsika Instituut, spetsialist

Teadustegevus

Aerosooliseadmete kalibratsiooni meetodite ja aparatuuri uurimine ning arendus.

DISSERTATIONES PHYSICAE
UNIVERSITATIS TARTUENSIS

1. **Andrus Ausmees.** XUV-induced electron emission and electron-phonon interaction in alkali halides. Tartu, 1991.
2. **Heiki Sõnajalg.** Shaping and recalling of light pulses by optical elements based on spectral hole burning. Tartu, 1991.
3. **Sergei Savihhin.** Ultrafast dynamics of F-centers and bound excitons from picosecond spectroscopy data. Tartu, 1991.
4. **Ergo Nõmmiste.** Leelishalogeniidide röntgenelektronemissioon kiiritamisel footonitega energiaga 70–140 eV. Tartu, 1991.
5. **Margus Rätsep.** Spectral gratings and their relaxation in some low-temperature impurity-doped glasses and chrystals. Tartu, 1991.
6. **Tõnu Pullerits.** Primary energy transfer in photosynthesis. Model calculations. Tartu, 1991.
7. **Olev Saks.** Attoampri diapasoonis voolude mõõtmise füüsikalised alused. Tartu, 1991.
8. **Andres Virro.** AlGaAsSb/GaSb heterostructure injection lasers. Tartu, 1991.
9. **Hans Korge.** Investigation of negative point discharge in pure nitrogen at atmospheric pressure. Tartu, 1992.
10. **Jüri Maksimov.** Nonlinear generation of laser VUV radiation for high-resolution spectroscopy. Tartu, 1992.
11. **Mark Aizengendler.** Photostimulated transformation of aggregate defects and spectral hole burning in a neutron-irradiated sapphire. Tartu, 1992.
12. **Hele Siimon.** Atomic layer molecular beam epitaxy of A^2B^6 compounds described on the basis of kinetic equations model. Tartu, 1992.
13. **Tõnu Reinot.** The kinetics of polariton luminescence, energy transfer and relaxation in anthracene. Tartu, 1992.
14. **Toomas Rõõm.** Paramagnetic H^{2-} and F^+ centers in CaO crystals: spectra, relaxation and recombination luminescence. Tallinn, 1993.
15. **Erko Jalviste.** Laser spectroscopy of some jet-cooled organic molecules. Tartu, 1993.
16. **Alvo Aabloo.** Studies of crystalline celluloses using potential energy calculations. Tartu, 1994.
17. **Peeter Paris.** Initiation of corona pulses. Tartu, 1994.
18. **Павел Рубин.** Локальные дефектные состояния в CuO_2 плоскостях высокотемпературных сверхпроводников. Тарту, 1994.
19. **Olavi Ollikainen.** Applications of persistent spectral hole burning in ultrafast optical neural networks, time-resolved spectroscopy and holographic interferometry. Tartu, 1996.
20. **Ülo Mets.** Methodological aspects of fluorescence correlation spectroscopy. Tartu, 1996.
21. **Mikhail Danilkin.** Interaction of intrinsic and impurity defects in CaS:Eu luminophors. Tartu, 1997.

22. **Ирина Кудрявцева.** Создание и стабилизация дефектов в кристаллах KBr, KCl, RbCl при облучении ВУФ-радиацией. Тарту, 1997.

23. **Andres Osvet.** Photochromic properties of radiation-induced defects in diamond. Tartu, 1998.

24. **Jüri Örd.** Classical and quantum aspects of geodesic multiplication. Tartu, 1998.

25. **Priit Sarv.** High resolution solid-state NMR studies of zeolites. Tartu, 1998.

26. **Сергей Долгов.** Электронные возбуждения и дефектообразование в некоторых оксидах металлов. Тарту, 1998.

27. **Kaupo Kukli.** Atomic layer deposition of artificially structured dielectric materials. Tartu, 1999.

28. **Ivo Heinmaa.** Nuclear resonance studies of local structure in $RBa_2Cu_3O_{6+x}$ compounds. Tartu, 1999.

29. **Aleksander Shelkan.** Hole states in CuO_2 planes of high temperature superconducting materials. Tartu, 1999.

30. **Dmitri Nevedrov.** Nonlinear effects in quantum lattices. Tartu, 1999.

31. **Rein Ruus.** Collapse of 3d (4f) orbitals in 2p (3d) excited configurations and its effect on the x-ray and electron spectra. Tartu, 1999.

32. **Valter Zazubovich.** Local relaxation in incommensurate and glassy solids studied by Spectral Hole Burning. Tartu, 1999.

33. **Indrek Reimand.** Picosecond dynamics of optical excitations in GaAs and other excitonic systems. Tartu, 2000.

34. **Vladimir Babin.** Spectroscopy of exciton states in some halide macro- and nanocrystals. Tartu, 2001.

35. **Toomas Plank.** Positive corona at combined DC and AC voltage. Tartu, 2001.

36. **Kristjan Leiger.** Pressure-induced effects in inhomogeneous spectra of doped solids. Tartu, 2002.

37. **Helle Kaasik.** Nonperturbative theory of multiphonon vibrational relaxation and nonradiative transitions. Tartu, 2002.

38. **Tõnu Laas.** Propagation of waves in curved spacetimes. Tartu, 2002.

39. **Rünno Lõhmus.** Application of novel hybrid methods in SPM studies of nanostructural materials. Tartu, 2002.

40. **Kaido Reivelt.** Optical implementation of propagation-invariant pulsed free-space wave fields. Tartu, 2003.

41. **Heiki Kasemägi.** The effect of nanoparticle additives on lithium-ion mobility in a polymer electrolyte. Tartu, 2003.

42. **Villu Repän.** Low current mode of negative corona. Tartu, 2004.

43. **Алексей Котлов.** Оксианионные диэлектрические кристаллы: зонная структура и электронные возбуждения. Tartu, 2004.

44. **Jaak Talts.** Continuous non-invasive blood pressure measurement: comparative and methodological studies of the differential servo-oscillometric method. Tartu, 2004.

45. **Margus Saal.** Studies of pre-big bang and braneworld cosmology. Tartu, 2004.

46. **Eduard Gerškevitš.** Dose to bone marrow and leukaemia risk in external beam radiotherapy of prostate cancer. Tartu, 2005.
47. **Sergey Shchemelyov.** Sum-frequency generation and multiphoton ionization in xenon under excitation by conical laser beams. Tartu, 2006.
48. **Valter Kiisk.** Optical investigation of metal-oxide thin films. Tartu, 2006.
49. **Jaan Aarik.** Atomic layer deposition of titanium, zirconium and hafnium dioxides: growth mechanisms and properties of thin films. Tartu, 2007.
50. **Astrid Rekker.** Colored-noise-controlled anomalous transport and phase transitions in complex systems. Tartu, 2007.
51. **Andres Punning.** Electromechanical characterization of ionic polymer-metal composite sensing actuators. Tartu, 2007.
52. **Indrek Jõgi.** Conduction mechanisms in thin atomic layer deposited films containing TiO_2. Tartu, 2007.
53. **Aleksei Krasnikov.** Luminescence and defects creation processes in lead tungstate crystals. Tartu, 2007.
54. **Küllike Rägo.** Superconducting properties of MgB_2 in a scenario with intra- and interband pairing channels. Tartu, 2008.
55. **Els Heinsalu.** Normal and anomalously slow diffusion under external fields. Tartu, 2008.
56. **Kuno Kooser.** Soft x-ray induced radiative and nonradiative core-hole decay processes in thin films and solids. Tartu, 2008.
57. **Vadim Boltrushko.** Theory of vibronic transitions with strong nonlinear vibronic interaction in solids. Tartu, 2008.
58. **Andi Hektor.** Neutrino Physics beyond the Standard Model. Tartu, 2008.
59. **Raavo Josepson.** Photoinduced field-assisted electron emission into gases. Tartu, 2008.
60. **Martti Pärs.** Study of spontaneous and photoinduced processes in molecular solids using high-resolution optical spectroscopy. Tartu, 2008.
61. **Kristjan Kannike.** Implications of neutrino masses. Tartu, 2008.
62. **Vigen Issahhanjan.** Hole and interstitial centres in radiation-resistant MgO single crystals. Tartu, 2008.
63. **Veera Krasnenko.** Computational modeling of fluorescent proteins. Tartu, 2008.
64. **Mait Müntel.** Detection of doubly charged higgs boson in the CMS detector. Tartu, 2008.
65. **Kalle Kepler.** Optimisation of patient doses and image quality in diagnostic radiology. Tartu, 2009.
66. **Jüri Raud.** Study of negative glow and positive column regions of capillary HF discharge. Tartu, 2009.
67. **Sven Lange.** Spectroscopic and phase-stabilisation properties of pure and rare-earth ions activated ZrO_2 and HfO_2. Tartu, 2010.
68. **Aarne Kasikov.** Optical characterization of inhomogeneous thin films. Tartu, 2010.

69. **Heli Valtna-Lukner.** Superluminally propagating localized optical pulses. Tartu, 2010.
70. **Artjom Vargunin.** Stochastic and deterministic features of ordering in the systems with a phase transition. Tartu, 2010.
71. **Hannes Liivat.** Probing new physics in e+e− annihilations into heavy particles via spin orientation effects. Tartu, 2010.
72. **Tanel Mullari.** On the second order relativistic deviation equation and its applications. Tartu, 2010.
73. **Aleksandr Lissovski.** Pulsed high-pressure discharge in argon: spectroscopic diagnostics, modeling and development. Tartu, 2010.
74. **Aile Tamm.** Atomic layer deposition of high-permittivity insulators from cyclopentadienyl-based precursors. Tartu, 2010.